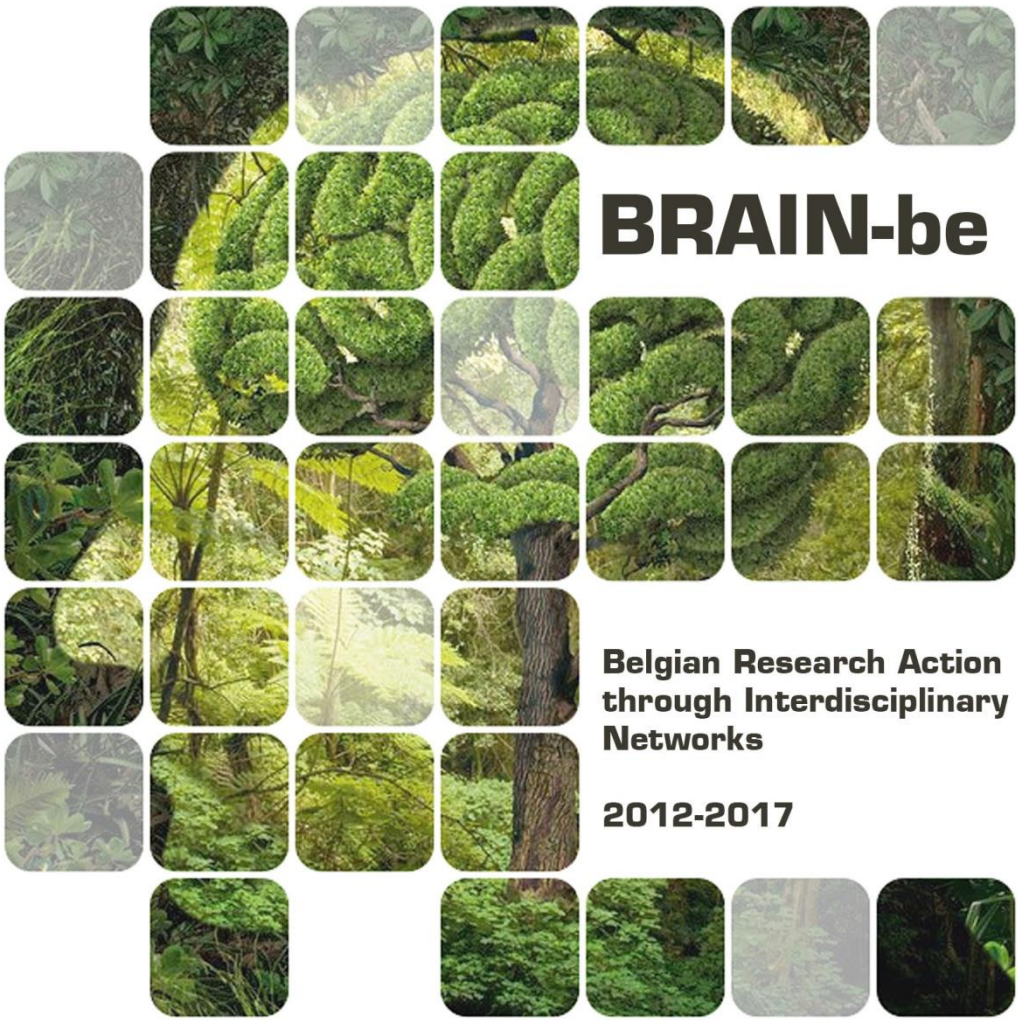

BR/175/A2/Chicxulub

Project Acronym CHICXULUB: Chicxulub 2016 IODP-ICDP deep drilling: From cratering to mass extinction

Period: Final Report (2017-2022)

Philippe Claeys (VUB) – Pascal Godefroit (RBINS) – Ozgur Karatekin (ROB)

Axis 2: Geosystems, universe and climate

belspo .be

NETWORK PROJECT

Project Acronym CHICXULUB:
Chicxulub 2016 IODP-ICDP deep drilling: From cratering to mass extinction

Period: Final Report (2017-2022)

Contract - BR/175/A2

FINAL REPORT

PROMOTORS: Philippe Claeys (VUB)
Pascal Godefroit (RBINS)
Ozgur Karatekin (ROB)
...

AUTHORS: Philippe Claeys (VUB)
Pascal Godefroit (RBINS)
Stijn Goolaerts (RBINS)
Ozgur Karatekin (ROB)
Cem Berk Senel1 (ROB)

museum VUB AMGC ORB - KSB belspo .be

Published in 2022 by the Belgian Science Policy Office
WTCIII
Simon Bolivarlaan 30 Boulevard Simon Bolivar
B-1000 Brussels
Belgium
Tel: +32 (0)2 238 34 11
http://www.belspo.be
http://www.belspo.be/brain-be

Contact person: Koen Lefever
Tel: +32 (0)2 238 35 51

Ph. Claeys, P. Godefroit, S. Goolaerts, O. Karatekin, C. Berk Senel1 (ROB), ***Chicxulub 2016 IODP-ICDP deep drilling: From cratering to mass extinction***. Final Report. Brussels: Belgian Science Policy Office 2022 – 59 p. (BRAIN-be - (Belgian Research Action through Interdisciplinary Networks)

TABLE OF CONTENTS

ABSTRACT

Context: This final report illustrates the succession of events that took place across the Cretaceous-Paleogene (K-Pg) boundary, 66 million years ago, exploiting the ~ 1300 m long core drilled by the joint International Ocean Discovery Program (IODP) – International Continental Scientific Drilling Project (ICDP) within the central part of the Chicxulub crater (~200 km) in Yucatan in 2016. Each work-package is described in details and the main conclusions of the study are highlighted. A section is also devoted to the list of scientific output (publications) and one to the actions carried out in terms of outreach, media, and communication towards a larger audience.

Objectives: Chicxulub had five objectives, each carried within a work package.

1) First objective: Reaction of the terrestrial lithosphere to a large cratering event, and the production/distribution of ejecta – WORK PACKAGE 1 –

2) *Second objective*: simulate this energy transfer to the Earth system via the atmosphere through a global atmospheric model – WORK PACKAGE 2 –

3) *Third objective*: test the link between the Chicxulub crater formation and the Deccan eruption peak at the K-Pg – WORK PACKAGE 3 –

4) *Fourth objective*: impact on latest Cretaceous terrestrial faunas in Europe and Asia – WORK PACKAGE 4 –

5) *Fifth objective*: compilation of objectives 1 to 4 to document the effect of impact and volcanism on the evolution of planets, mantle, and atmosphere – WORK PACKAGE 5 –

Conclusions: The report describes the thick sequence of impactites, and shocked basement lithologies recovered by the IODP-ICDP large-scale international endeavor in terms of petrography, geochemistry, shock metamorphism, emplacement, origin etc. This approach leads major progress in the understanding of the crater formation process; with a particular emphasis on the formation of the central peak-ring structure, the distribution of melt, and the formation of ejecta. Detailed examination of the IODP-ICDP material better documents the proportion of dust, carbonates and evaporates implicated in the cratering event. The crater excavation process let to the release of large volumes of CO_2, SO_x and H_2Ov by shock vaporization of carbonates and evaporites composing the upper 3 km of Yucatan target rock at time of impact, combined with that of huge amounts of fine silicate dust produced by the underlaying basement lithologies. The release over a very short timescale of these components played a key role in the resulting global perturbation of the atmosphere and ultimately the mass extinction, including the demise of the dinosaurs. A new global climate model that better simulate this perturbation document major temperature changes all over the Earth after the collision is presented with a special accent on the role of fine silicate dust. This study also describes the consequences of this event on specific components of the Cretaceous biosphere

Keywords: impact-cratering, mass-extinction, flood- volcanism, mantle-dynamics, terrestrial-analogue

1. INTRODUCTION

A large asteroid or comet impact took place 66 million years ago at the Cretaceous-Paleogene (K-Pg) boundary. This collision formed the ± 200 km in size Chicxulub crater, in Yucatan (Mexico), and likely contributed to the K-Pg mass extinction, which saw the demise of the non-avian dinosaurs together with 60-70% of the Earth fauna and flora. The 1335-m long core recovered offshore Yucatan in April 2016, by the IODP-ICDP drilling located within the peak-ring zone of the Chicxulub crater is examined in detail. The "kill mechanisms" commonly invoked for the impact causation of extinctions involve release of large volumes of volatiles, dust, aerosols and particulates into the atmosphere. These components were released via the shock vaporization of the carbonate and evaporite sediments (CO_2, SO_x, H_2O_v that composed the upper 3 km of the Yucatan target rock and fine pulverized dust from the underlying basement. In both cases, they appear capable of major environmental degradation depending upon the timescales of emission(s) and the efficiency with which volatiles are delivered to the stratosphere. This report describes the significant advances made in our understanding of the cratering process (crust – lithosphere objectives 1 & 2), documents using a modeling approach the effects of on the global Earth system (atmosphere – hydrosphere – biosphere perturbation objectives 2, 4, 5) that lead to the K-Pg mass extinction and investigates the reponses of the biosphere to this major perturbation. The results produced are directly relevant and in full compliance with this 2016 BRAIN call to study the dynamic of planet Earth.

2. STATE OF THE ART & OBJECTIVES OF THE PROJECT

A review paper of 30 years K-Pg research, published in Science [Schulte et al. 2010] set the stage for this BELSPO project. In 1980, the hypothesis that a meteorite impact caused the end Cretaceous mass extinction and the demise of the dinosaurs 66 million years ago stirred up geology [Alvarez et al. 1980; Smit et al. 1980]. It relied on a positive iridium anomaly detected in the fine clay layer that marks the boundary between the Cretaceous and the Paleogene (K-Pg boundary, previously K-T for Kreide-Tertiaire). This hypothesis gained support by the discovery in the boundary clay of shocked quartz, testifying of dynamic pressures way above 5 GPa [Bohor et al. 1984], which only occur by impact cratering or nuclear testing and highly oxidized Ni-rich magnesioferrite spinels [Smit and Kyte, 1984], similar as to the ones found in meteorite fusion crust. In 1990, the smoking gun was found with the identification of Chicxulub crater, now buried 1000 m under the Yucatan peninsula and the Gulf of Mexico, which is timely and genetically linked to the K-Pg boundary [Hildebrand et al., 1990; Swisher et al. 1992]. Finding the crater, tilted the balance in favor of the impact scenario in the ongoing debate with the opposing hypothesis of a global climate and biosphere perturbation generated by the emplacement of the huge Deccan basalts in India (~106 km3). Recently, it was suggested that Chicxulub-induced dynamic stress and seismicity stimulated the Deccan magma chamber, triggering major pulses of volcanism that hampered post-extinction recovery of ecosystems [Renne et al. 2015; Richards et al. 2015]. During the 1990s, geophysical studies documented the morphology and size of Chicxulub showing a well-preserved impact structure [Morgan et al. 1997; Morgan and Warner, 1999]. The recent IODP-ICDP drilling further refined the structure and morphology of the central peak-ring [Morgan et al. 2016; see also annual report 2019]. Rare core fragments (from old 1970 Pemex oil exploration wells), clearly demonstrated the impact origin, dated the melt-lithologies to be of K-Pg age and characterized the target rock [Swisher et al. 1992]. In parallel, studies unequivocally linked the ejecta found with the K-Pg boundary layer at proximal sites to the Chicxulub crater [Alvarez et al. 1992; Smit et al. 1992]. Climate models illustrated the possible effects of the volatiles released by the event on the chemistry of the atmosphere [Pierazzo et al. 1998; Pierazzo & Artemieva, 2012]. Geophysical data showed that Chicxulub was a unique structure not only because of its potential environmental effects but also as a well-preserved terrestrial analog to the many craters observed on the Moon, Mars, and other solar system bodies. With a diameter around 200 km Chicxulub falls within the transition between a peak-ring and a multi-ring basin, such as Orientale (910 km) on the Moon. The crustal deformation processes leading on Earth and other planetary bodies to the formation multi-ring basins remain complex and not fully understood [Urrutia et al. 2004]. However, the highly shocked, sheared, and foliated state of the granite recovered by the IODP-ICDP drilling, now clearly point towards a formation according to the dynamic collapse model with rock flow, with a brief period of catastrophic rock weakening and acoustic fluidization, during intense uplift, followed by rapid increase in strength to sustain the topographic rings. [Morgan et al. 2016; Riller et al. 2018]. As Chicxulub is one of the only terrestrial craters with a well-defined and well-preserved “peak-ring” and a complete ejecta sequence, it can now be used to learn about large crater formation on solid planetary surfaces, with major consequences for ongoing planetary and rover missions to Mars and other bodies (ex. DART mission). Clearly, the new knowledge gained on Chicxulub constitutes an asset for space missions like ESA/NASA Asteroid Impact and Deflection Assessment (AIDA) collaboration composed of EAS/HERA and NASA/DART missions, or to understand role played by impact on the evolution of early Mars, 4 billion years ago.

In April 2016, IODP drilled the Chicxulub crater offshore as a joint venture with ICDP (see http://www.eso.ecord.org/expeditions/364/364.php). This BELSPO project based on the recovered core within the crater, and more than 30 years of K-Pg research, included the following objectives:

1) use the new core to document the cratering process, peak-ring formation, and the products injected into the atmosphere that likely led to the mass extinction,
2) simulate the energy transfer to the Earth system using an ROB developed atmospheric model,
3) test the hypothesis the dynamic stress from Chicxulub impact intensified Deccan trap volcanism, **which was not possible due to Covid banning travel to India.**
4) better evaluate the reaction of Earth fauna and flora, with a particular emphasis on terrestrial vertebrates through the study of new latest Cretaceous fossil localities in key localities in Europe and Asia,
5) learn from Chicxulub to understand the evolution of terrestrial planets, including the consequences of large impacts on mantle and atmosphere evolution.

Major results and outcome of the project are presented in the following pages. More information and details can be found in the peer-reviewed publications listed at the end of this report.

3. METHODOLOGY AND MAJOR RESULTS

3.1) First objective: Reaction of the terrestrial lithosphere to a large cratering event, and the production/distribution of ejecta – *Work Package 1*

3.1.1) Introduction

The IODP-364-M0077 core was studied at the VUB using petrographic thin sections, SEM/EDX, µXRF, IRMS, HR-ICP-MS and MC-ICP-MS. Drill core M0077A samples the peak ring of Chicxulub offshore the Yucatán Peninsula (Fig. 1). Main focus lies on the 1) Suevite – Paleogene transition (core 40-1, [Goderis et al. 2021]); 2) entire suevite and impact melt rock sequence (Upper Peak ring section, *PhD thesis Pim Kaskes, expected to graduate Winter 2023*)' 3) granitic peak ring rocks intruded by pre-impact dikes and intercalated with suevites and impact melt rocks (Lower Peak Ring section, *PhD thesis Sietze de Graaff, April 2022)* and vaporization processes (PhD Thomas Déhais, *expected to graduate Winter 2022*).

The current results are summarized on the following pages. The VUB-AMGC group provided the geochemistry/petrography/isotopic data used in several papers published by the IODP-ICDP 364 team in 2017-2022 (see publication list). Several papers focusing on the results illustrated below have been published by the VUB team as first authors, and several others have been submitted or are being finalized for submission before end of 2022.

3.1.2) Impactites study to derive an emplacement mechanism of the different units.

The core examined within this project is illustrated in Figure 1.

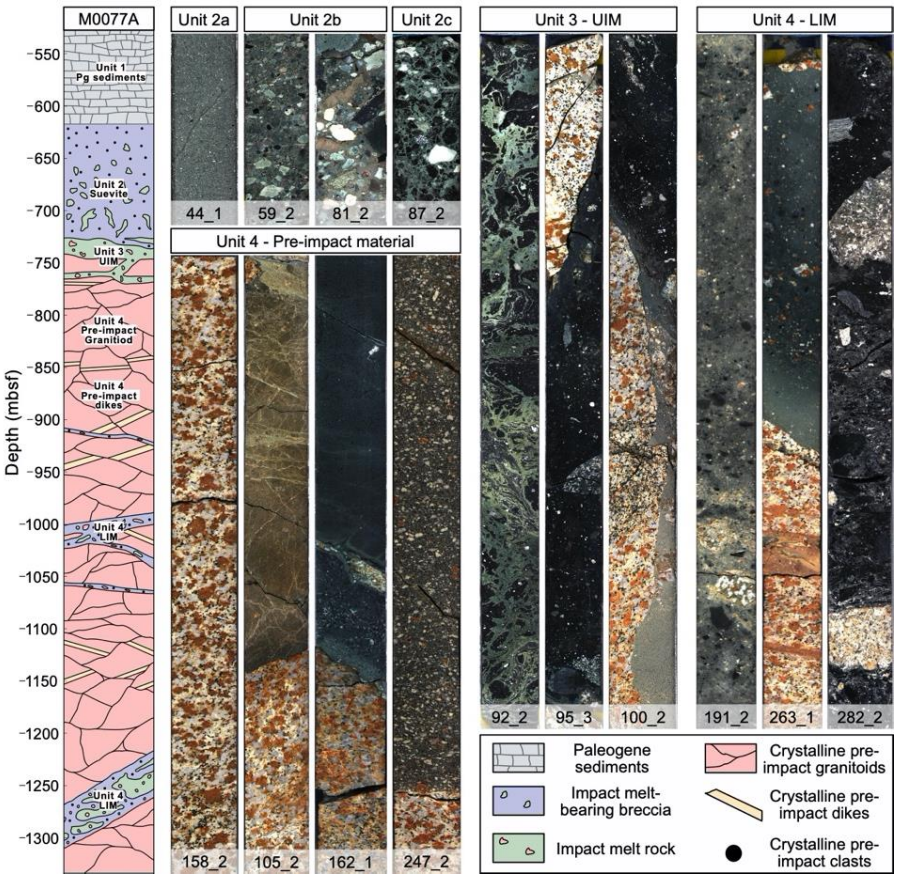

Figure 1. Hole M0077A core overview (width 83 mm) with representative core sections. *Unit 2*, showing the variation in the suevite unit with depth; *Unit 3*, showing the variation from green schlieren and black melt (UIM) to black melt with clasts and black melt with basement interaction; *Unit 4* – LIM, showing the variation from greyish to more blackish melt; *Unit 4* – pre-impact material, showing, from left to right, granitoid (158_2), felsite (105_2), dolerite (162_1) and dacite (247_2). UIM = upper impact melt rock, LIM = lower impact melt rock. Post-impact unit-1 is not discussed here. (De Graaff et al. 2022)

Petrography and geochemistry of the suevite (unit 2) and melt-rock (unit 3) from the peak-ring identifies the target components, their relative proportion within the impact melts were examined in detail. First focus was the transition between the suevite and unit 1 the Paleogene that overlies the impactites. This transition occurs over ± 1 m in core 40R-1.

3.1.3) Identification of the positive Ir anomaly within the peak-ring sequence of Chicxulub

A major finding carried out by the AMGC-VUB group was the discovery of the famous positive platinum group anomaly, which is recorded all over the world at the K-Pg boundary, also within the Chicxulub crater peak-ring sequence in IODP-ICDP- hole M0077A (Goderis et al. 2021, contact unit 1-2 in Fig. 2). The highest concentration of ultrafine meteoritic matter marked by elevated Ir concentration around (± 1 ppb) occurs in the post-impact sediments that cover the crater peak ring, just below the appearance of the lowermost Danian pelagic limestone. The following scenario is put forward: years to decades after the impact event, this part of the Chicxulub impact basin returned to a relatively low-energy depositional environment, recording in unprecedented detail the recovery of life during the succeeding millennia and the slow settling of the PGE anomaly. The iridium layer provides a key temporal horizon precisely and definitively linking Chicxulub to K-Pg boundary sections worldwide (Goderis et al. 2021).

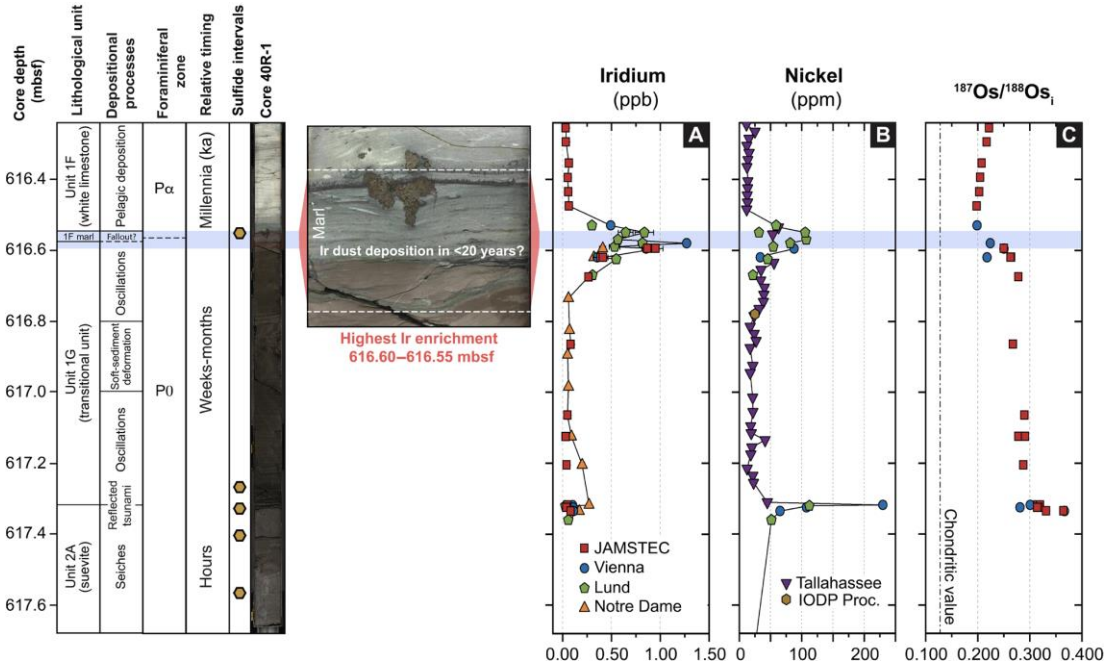

Figure 2. Chemostratigraphy of Core 40R-1. Profile of iridium concentrations (A), nickel concentrations (B), and initial 187Os/188Os (C) relative to lithological units. Symbol legends designate the laboratories where the respective siderophile element concentrations were determined. Uncertainties on Ir concentrations and $^{187}Os/^{188}Os$ are expressed as 2 SE or 2sigma for data determined by mass spectrometry and instrumental neutron activation analysis iridium coincidence spectrometry, respectively (mostly contained within the symbols). The interval of highest Ir enrichment is highlighted in blue, which corresponds to the white dashed lines in the enlarged core photograph. The high-resolution line scan photo is from the onshore science party. While the siderophile element enrichment in the gray-green marlstone and at the top of the transitional unit reflects the deposition of meteoritic matter, the elevated concentrations at the bottom of the transitional unit result from sulfide mineralization following hydrothermal activity in the impact basin. The highest HSE enrichment at the base of the gray-green marlstone (~616.58 mbsf) is interpreted to record the settling of Ir-rich dust, estimated to have been deposited within a few decades after the impact event, and subsequently reworked into a broader interval. (Goderis et al. 2021)

3.1.4) The suevite composition and geochemistry

Throughout the 104 m of stratigraphy, a polymict breccia with a particulate, fine-grained matrix was detected with abundant altered glass fragments (in general >50%). This suevite and in particular, the glass shards, now mostly replaced by phyllosilicate minerals, show varying degrees of alteration throughout the core. The Exp. 364 suevite is characterized by a fining and increasingly well-sorted upward trend. Based on our petrographic observations and µXRF maps, the suevite is subdivided in at least four general intervals (Fig. 3).

Interval 1 (core 40 to core 49): a relatively well sorted, fine-grained (>5mm), matrix supported suevite with isolated foraminifera, small carbonate and chert clasts and a brown micritic matrix. Abundant angular brown glass fragments altered to phyllosilicate minerals are present, and no basement clasts are found.

Interval 2 (core 49 to core 59): a poorly sorted, medium to coarse grained (~5-10 mm), matrix-supported suevite with abundant green-yellowish, vesicular melt particles and few angular chert fragments. No isolated microfossils are found in the matrix, only within limestone clasts, together with fragments of large macrofossils such as corals.

Interval 3 (core 59 to core 80): a poorly sorted, coarse-grained unit (~5-20 mm) with the first clear basement clasts, which are dominated by granitoids with some rare gneisses. This unit appears to be often clast-supported and displays pervasive hydrothermal alteration, clearly visible in the alteration rims of vesicular melt particles.

Interval 4 (core 80 to core 87): a very poorly sorted, matrix-supported suevite, which is intersected by dark impact melt bodies. The matrix of the suevite is not micritic, but clastic and Ca rich (Fig. 1). Many vesicular, equant melt shards are present together with large basement clasts and recrystallized carbonate clasts.

In contrast to these petrographic observations, the suevite displays a rather homogeneous major elemental composition, with a slight increase in CaO content towards the top (Fig. 3). The observed variations downcore are mostly related to increasing clast size. The bulk trace elemental composition of the suevite is similar to that of the upper and lower impact melt, although the suevite show an enrichment in Sr. Based on bulk µXRF trace element data, the suevite sequence is characterized by a very low S content (<0.7 wt%), the only outliers occurring close to the transitional unit and in an interval rich in large carbonate clasts (Fig. 1). The S-rich minerals in these intervals that were characterized using µXRF have petrographically been identified as being pyrites (FeS_2), and not as anhydrite ($CaSO_4$), gypsum ($CaSO_4$*H2O), or other types of iron sulfides (e.g., marcasite). Most melt particles analyzed using µXRF spot analysis show a basaltic to andesitic composition, with little variation with depth. This is verified and refined with Electron Microprobe Analysis and Laser Ablation ICP-MS measurement campaigns, following a strategy carried out on previous Chicxulub cores, such as Yaxcopoil-1 melt particles.

The characteristics described above show an influence of fragments from the carbonate platform (limestone & chert) within the entire suevite unit in contrast to the felsic basement, which seems not to have affected the deposition of intervals 1 and 2. The well-sorted uppermost ~ 30 m of the suevite (core 40 to 49), which is characterized by isolated foraminifera and higher CaO content, suggests that ocean water resurge in the crater caused settling and sorting of the clasts. The emplacement of the middle and lower part of the suevite is more difficult to interpret due to pervasive hydrothermal alteration.

The absence of S and lack of anhydrite clasts observed in the entire Exp. 364 suevite is not something that was witnessed to that extent in other Yucatán boreholes. For example, the suevite from the Yucatán-6 core shows some large anhydrite clasts in the lower interval, but the evaporite-carbonate ratio does not exceed 20%. Bulk µXRF S-values of samples from Yucatán-6 range from 0.2-3.7 wt%. In addition, impact breccias from the lower part of core UNAM-5, ~ 20 km outside of the crater, are rich in anhydrite clasts and show S-values between 16-23 wt%. These differences in S and amount of anhydrite clasts might be explained by the location of the Exp. 364 core on the Chicxulub peak ring. It is interpreted that in the peak ring zone, massive shock-vaporization of the pre-impact evaporite platform could have occurred or a particle size effect removed large parts of this cover.

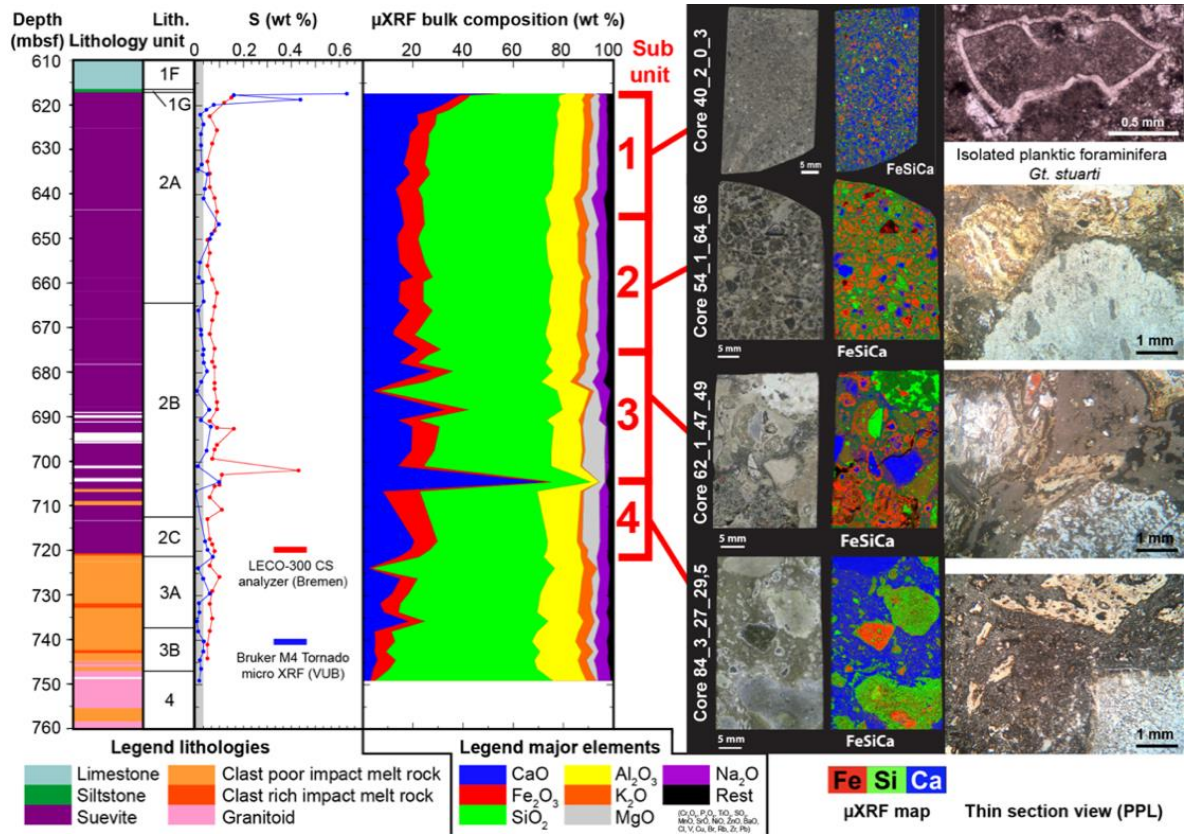

Figure 3. Bulk major elemental composition of the upper peak ring interval of IODP-ICDP 364 core determined by µXRF at AMGC-VUB, together with µXRF elemental maps of representative samples, and petrographic images covering the suevite stratigraphy. [modified from Gulick et al. 2019]

3.1.5) Granite composition and characterization

The granites are characterized by high SiO_2 (~70 - 78 wt%) and low MgO (< 1.5 wt%) contents (Fig. 1) and show an enriched light rare earth element signature when compared to CI chondritic composition, with most plotting above 10x CI, while heavy rare earths show values below 10x (Fig. 4). This results in strongly varying La/Yb ratios from 10 up to 50x CI (Fig. 5). Their composition is homogeneous throughout the stratigraphy, arguing for lateral consistency of the granites. The more mafic dolerites, with low SiO2 (~43 - 50 wt%) and high MgO (~9 - 15 wt%) contents, display a flatter trace element pattern, between 10 and 100x CI. With one exception, the La/Yb ratios are, comparatively low, not being higher than 5. The felsites and dacites are distinct from one another, with the former representing the more enriched lithology, showing trace element values of around 100x CI up to 1000x and La/Yb

ratios up to 30. While the dacites do show similarly high La/Yb ratios, their overall trace pattern is less enriched than the felsite

Geochemical variations in the impact melt rocks highlight the complex nature of the impactites, and its formation process. This is documented in the higher Al_2O_3 (up to 18 wt%) and CaO (up to 20 wt%), and generally lower Fe_2O_3 and MgO (around 5 and 2 wt%, respectively) contents of the upper relative to the lower impact melt rocks. However, the trace element compositions of both the upper and lower impact melt rocks are quite similar (Fig. 4). Interestingly, they are also comparable to those in the suevite [Kaskes et al. 2022]. Slight variations, such as Sr and Ca enrichment in the suevite, likely reflect the contribution of carbonate material (i.e., as clasts and/or matrix). These variations notwithstanding, these observations suggest large scale homogenization of the Chicxulub impactite material [De Graaff et al. 2022].

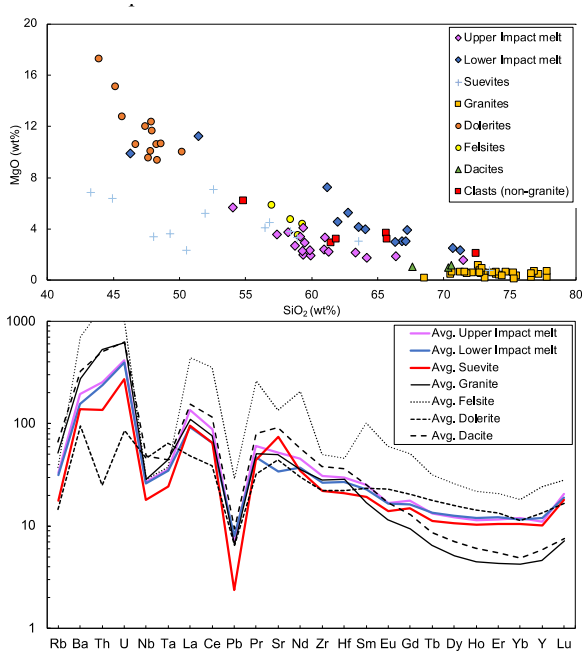

Figure 4. Mg vs SiO_2 with data recalculated on a volatile-free basis (top). CI Chondrite-normalized trace element data of reported lithologies.

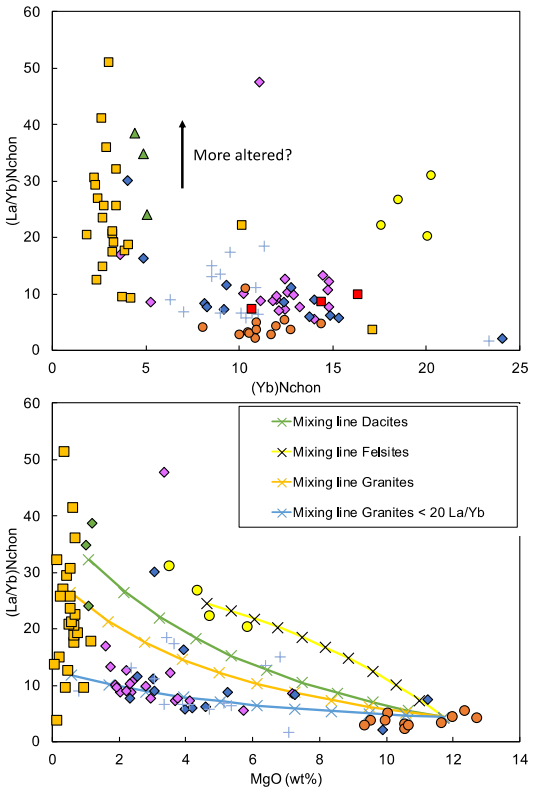

Figure 5. CI Chondrite-normalized La/Yb plotted versus Yb (top) and MgO (bottom). MgO is recalculated on volatile-free basis. Mixing lines are calculated between averaged dolerites and averaged (possible) endmembers. Symbols as in Fig. 4

Even though most trace element contents appear highly comparable, specific trace element ratios allow for better disentanglement of the impact melt components. Figure 5 shows mixing lines calculated between the dolerites and all pre-impact material. Mixing of averaged granites, felsites, and dacites with averaged dolerites, is not able to resolve the low La/Yb ratios observed in the impact melt [Fig. 5]. Only mixing between averaged granites that have < 20 La/Yb can explain the low ratios observed in the impact melt rocks [Fig. 5]. These observations imply one of the following scenarios: (1) The impact melt rocks represent the

residue of a differentiated impact melt, recorded by the high Yb compared to La (Fig. 5); (2) An unconstrained target rock component significantly contributed to the melt that drove up Yb (to conversely decrease the La/Yb). Such contribution may derive from the non- granitic, crystalline and/or metamorphic clasts that have been documented to occur in the Chicxulub impact melt rocks; (3) Alternatively, granites with La/Yb ratios of less than 20 represent less altered material, suggesting most of the granites to be significantly altered. Pervasive alteration has affected the Chicxulub core with Ca-Na and K-metasomatism potentially compromising whole rock compositions of fluid-mobile elements (including La, Na, K). Consequently, variations in such elements might reflect alteration rather than primary magmatic signals. The observation that La/Yb ratios of the granites display variations by a factor of ~5 at similar Yb compositions (Fig. 5) strongly suggests that La has been remobilized, with only granites exhibiting La/Yb < 20 preserving primary signatures. This is also supported by La/Yb ratios plotted versus immobile elements Ti and Zr, wherein La/Yb is decoupled from variations in both elements [see De Graaff et al. 2022 for more details]. Feignon et al. (2021) classified the granite (unit 4) as part of high-K, calc-alkaline metaluminous series, characterized by high Sr/Y and (La/Yb) ratios, and low Y and Yb contents, which are typical for adakites. The $^{87}Sr/^{86}Sr$ is indicative of a hydrothermal overprint; while the epsilon Nd (t=326 Ma) values indicate a moderately enriched crustal material in the source region involved in the granite genesis.

3.1.6) Emplacement process(es) of the different units

In short, basement felsic and mafic lithologies mixed as part of an initial large melt pool, with varying degree of $CaCO_3$ contribution, and then separated in the final crater formation phase; the lower impact was injected into the underlying basement, while the more $CaCO_3$-rich melts remained at the "top" of the rising peak-ring [De Graaff et al. 2022]. In parallel, the overlying suevite (unit 2 in figure 3 above) is described in Kaskes et al. (2022). The main points are: The suevite sequence is subdivided into several units that are distinct in their petrography, geochemistry, and sedimentology. All these suevite units have isolated Cretaceous planktic foraminifera within their clastic groundmass, which suggests the influence of marine processes. First, ocean water that reached the northern peak ring region entered through a N-NE gap in the Chicxulub outer rim. This water caused intense quench fragmentation when it interacted with the underlying hot impact melt rock, and this resulted in the emplacement of the ~5.6-m-thick hyaloclastite-like, non-graded suevite unit. In the following hours, the impact structure was flooded by an ocean resurge rich in rock debris, which caused the phreatomagmatic processes to stop and the ~89-m-thick graded suevite unit to be deposited. We interpret that after the energy of the resurge slowly dissipated, oscillating seiche waves took over the sedimentary regime and formed the ~3.5-m-thick bedded suevite unit. The final stages of the formation of the impactite sequence (estimated to be <20 years after impact) were dominated by resuspension and slow atmospheric settling, including the final deposition of Chicxulub impactor debris, with its Ir anomaly [Goderis et al. 2021].

3.1.7) The target rock lithologies and the evolution of the Gulf of Mexico before the impact.

The IODP drilling also shed light on the poorly understood and rarely outcropping pre-Mesozoic basement of the Maya block in Southern Mexico and Yucatan, on the tectonic evolution of this key terrane of the Gulf of Mexico and its relationships with Gondwana and Laurentia. Our petrography and geochemistry work on unit 3 and 4 identified intervals rich in zircons, which were analyzed at China Institute of Geosciences [Zhao et al. 2020; Zhao

et al., 2021] and University of Texas at Austin [Ross et al. 2022] for their chronologies. Zircon rare earth element chemistry support the formation of the granitoids within a continental arc context [de Graaff et al. 2022]. These zircons yielded a new set of ages clustered around 326±5 Ma, which likely represent the extension of Alleghanian granites known in the Southern Appalachia region [Zhao et al. 2020]. Along with the presence of new zircons ranging in ages from 317 and 345 Ma, inherited zircons fall into 3 groups, Peri-Gondwanan (400-435 Ma), Pan-African (500-636 Ma) and Oaxaquian (940 – 1400 Ma) [Ross et al. 2022]. The cored granite unit intruded the Maya block during the Carboniferous, in an arc setting with crustal melting related with the closure of the Rheic ocean associated with the assembly of Pangea.

3.2) Second objective: simulate this energy transfer to the Earth system via the atmosphere through a global atmospheric model – *Work Package 2* –

3.2.1) Introduction

The aim of this WP 2 was to contribute to the extensive debate as to the cause of the K-Pg mass extinction triggered by the formation of the Chicxulub in Yucatan by refining existing knowledge on the injection within the atmosphere of volatiles and dust released by the impact. It is important to model using state of the art approaches how the Chicxulub cratering event affected the atmosphere, the global earth system and the biosphere, to induce the brutal disappearance of organisms. Previous climate scenarios were put forward to show how the injection of dust, and gases, over short time scales (hours-days) affected the upper atmosphere [Pierazzo et al. 2012; Toon et al. 2016; Artemieva et al., 2017; Brugger et al. 2017; Tabor et al. 2020; Morgan et al. 2022]. The culprit is the ± 3 km thick sedimentary cover of the Yucatan target rock that was composed of carbonates ($CaCO_3$) and evaporites ($CaSO_4$), which by shock degassing likely released huge volumes of CO_2, SO_x and H_2O vapor into the atmosphere, together with fine pulverized silicate dust. These models vary significantly and strongly focus on the quantity of sulfur-rich volatiles released (ex. SO_X varies between 40 and 560 Gt). However, the production of fine-grained pulverized silicates (<<10 µm) from the upper part of the deeper Pan African basement received less attention. For WP 2, our working hypothesis and major focus was that the finely pulverized silicate-rich material is also a key component of the atmospheric perturbation. Moreover, we consider that this fine dust is somewhat analog to the finest fraction of the matrix present in lapilli ejecta from proximal sites and recovered in the upper impact breccia of Yucatan-6, in IODP-ICDP 364, and most of all to the finest grain fraction recovered at the Tanis K-Pg [Claeys et al. 2003; Kaskes et al. 2022, Senel et al. submitted]. Although somewhat neglected in previous models (see references above), this very fine silicate dust (nano & micro-scale) injected into the atmosphere, likely diminished the amount of light and energy received by the planet.

3.2.2) General circulation modeling (GCM) overview

To test the role of the fine dust, we developed a new paleoclimate GCM at ROB, which uses ROB paleoEarth implementation of the general-purpose the planetWRF model [Richardson et al. 2007] that has been widely applied and validated for planetary atmospheres [Temel et al. 2021; Senel et al. 2021]. The simulations were performed with the new model to explore the relative roles of impact generated aerosols on environment and, in particular, on photosynthetic activity [Senel et al submitted].

This novel paleoEarth model is a GCM specialized to simulate the Chicxulub impact at the K-Pg boundary, using the latest Cretaceous paleogeography for geographic boundary conditions and plant functional types for land surface conditions [Markwick and Valdes, 2004; Niezgodzki et al. 2017]. It resolves the atmospheric transport of fine-grained ejecta (i.e., consisting of sulfur, soot and silicate dust) generated by the Chicxulub impactor, considering the radiative and microphysical feedback of climate-active ejections. Regarding the verification of GCM, simulated pre-impact surface temperatures agree well with proxy-based latest Cretaceous temperature reconstructions. Moreover, in a recent inter-comparison study [Morgan et al., 2022], our initial GCM reconstructions for the post-impact global temperature drop fall in line with those of previous GCM simulations following the Chicxulub impact.

The paleoEarth GCM consists of three main components, besides the dynamical core of planetWRF. The first is a module implemented for the asteroid/cometary impact dynamics, in which the transport of impact-generated fine-grained ejecta is governed in the GCM. The second and third components are radiative transfer and microphysics modules, respectively.

A) Radiative transfer and microphysics modeling
This radiative transfer module considers the radiative effect of impact-ejecta, such as the absorption, reflection and scattering by ejected particles in the shortwave and longwave spectrum. It was built within the NASA Goddard shortwave/longwave radiation scheme [Chou & Suarez, 1999; Chou et al., 2001] that is composed of 8 spectral bands within the ultraviolet and visible range (< 700 nm) and 3 spectral bands in the infrared region (> 700 nm). In this component, specific extinction, single scattering albedo and asymmetry factor of sulphate were set as function of wavelengths in shortwave and longwave spectral bands. Regarding the dust, optical properties are specified following previous studies, in the shortwave and longwave spectrum, while for soot, they are determined in shortwave and longwave spectral bands [Dufresne et al. 2002; Hess et al. 1998; Binkowski & Shankar, 1995].

The microphysics module resolves the microphysical processes of fine-grained ejecta, such as dry and wet deposition processes of soot, sulfur and silicate dust. These processes are crucial in determining deposition rates, as a result, the lifetimes of deposited particles in the atmosphere. For the dry deposition modeling of soot and dust, our GCM considers relative contributions of gravitational and aerodynamic forcing as well as the Brownian diffusion, impaction, and interception of particles, using a particle-size aware resistance model [Binkowski & Shankar, 1995; Zhang & Shao, 2014; Emerson et al. 2020], i.e.,

$$V_d = V_g + \left(\mathcal{R}_a + \mathcal{R}_s + \mathcal{R}_a\mathcal{R}_s V_g\right)^{-1} \quad \text{(Eq. 1)}$$

where V_d and V_g are the deposition and gravitational settling velocities, while $\mathcal{R}_a$ and $\mathcal{R}_s$ are aerodynamic and surface deposition resistances. The latter term reads,

$$\mathcal{R}_s = \frac{1}{\epsilon_0 u_* (E_b + E_{im} + E_{in})} \quad \text{(Eq. 2)}$$

where $\epsilon_0 = 3$ is an empirical constant, u_* is the friction velocity of near-surface winds that GCM computes, E_b, E_{im} and E_{in} are collection efficiencies related to Brownian diffusion,

impaction and interception of particles determined from previous models. While the dry deposition rate of sufate was selected to prescribe by which the land deposition rate was set to 0.1 cm/s referring to the value of coniferous and deciduous forest covered land [Xu et al. 1998]. Likewise, the ocean deposition rate is prescribed to be 0.1 cm/s that falls in between 0.05 cm/s and 0.20 cm/s. Note that our sulfur cycle simulations do not include photochemistry reactions. We presumed that the sulfur injection is fully converted into sulfate as the maximum scenario, as sulfur has almost 3 to 4 times higher deposition rates on land and in the ocean, 0.6-0.8 cm/s **[**Feichter et al. 1998**]**, leading to faster deposition than sulfate.

Moreover, the wet deposition of particles is modeled by resolving in-cloud rainout and washout processes [Tsarpalis et al. 2018]. For the dust microphysical modeling, our GCM takes dust lifting into account, consisting mainly of three mechanisms: (i) dust lifting by aerodynamic forces, (ii) saltation bombardment and (iii) breakdown of large aggregates, i.e., disaggregation. Note that the microphysical modeling of soot and dust were implemented in a size-resolved way [Binkowski & Shankar, 1995] unlike the monodisperse assumption in sulfate modeling. Here, the size-resolved modeling follows both our recent two-moment dust transport scheme initially derived for the Martian dust cycle and a two-moment framework widely used in community atmosphere models **[**Binkowski & Shankar, 1995; Senel et al. 2021]. Our soot and dust microphysics models do not include coagulation microphysics which is necessary for extremely fine nanometric particle sizes below 0.1 µm, i.e., 0.015 µm < D_p < 0.052 µm (the Aitken mode**,** Liu et al. 2012). However, in our study, the median size of dust and soot particles are relatively large with a median grain-size of 0.125 µm and 0.22 µm, respectively (corresponding to the accumulation mode), so we assume the effect of coagulation to be minor on the overall atmospheric processes following the Chicxulub impact event.

B) Description of simulation set-up and model physics

For the land-surface physics, in our GCM simulations we made use of the five-layer thermal diffusion scheme. To model the water-cycle, cloud and precipitation microphysics, we used the Purdue-Lin microphysics scheme [Tiedtke, 1989]. The modified Tiedtke scheme is utilized for the cumulus parameterization and the planetary boundary-layer (PBL) turbulence is modeled by means of our recent PBL scheme [Senel et al. 2019]. The atmospheric surface layer is modeled by using the revised MM5 scheme [Jimemez et al. 2012]. Regarding the ocean modeling, we use the Pollard Ocean mixed layer model that accounts for the wind-driven turbulent mixing and deepening in the ocean [Davis et al., 2008].Moreover, we imposed the latest Cretaceous climatic conditions, taking global-average atmospheric CO_2 concentration to be 560 parts per million (ppm). For the orbital forcing, a circular orbit with an obliquity of 23.5° and a solar constant of ~1354 W/m^2 (i.e., faint young sun compared to present solar constant) are assumed, similar to other paleoclimate studies [Brugger et al. 2017]. The moment of the Chicxulub impact, thus the release of fine-grained ejecta, is assumed to be initialized in the boreal spring [During et al. 2022]. This assumption is based on recent osteohistological and isotopic studies from uniquely preserved fossil fish from the Tanis K-Pg site (the same we base our grain size analyses on), and this moment of impact likely significantly influenced selective biotic survival across the K-Pg boundary catastrophe. The horizontal model resolution of GCM is 5ºx5º over longitudinal and latitudinal directions, having 27 vertical sigma layers extending through the stratopause. Furthermore, the time-

integration for each impact simulation is carried out for 35 years following an initial spin-up simulation of 15-years, in which the latest Cretaceous conditions stabilized.

C) Calculation of photosynthetic active radiation flux

Photosynthetic active radiation or PAR flux refers to the solar radiation reaching the surface between the λ=400-700 nm spectral range, indicating how intense the radiative flux is to sustain photosynthesis [Pierrehumbert & Gaidos, 2011]. It is thus highly significant in quantifying the global primary production. In our paleoEarth GCM, the time evolution of global PAR flux is computed within the radiative transfer module at each model timestep. As the NASA Goddard shortwave/longwave radiation scheme solves the radiative transfer in spectral bands, the 8th spectral band corresponds to the PAR spectral range, in which we saved model results at each hour and post-processed this for detailed interpretations.

3.2.3) Results and discussion

The K-Pg impact winter-hypothesis, proposed originally in 1980 was centred around dust-sized material that was ejected from the crater into the stratosphere and subsequently spread around the globe [Alvarez et al. 1980]. However, this dust scenario was later rejected because the fraction and mass of this clastic debris at the K-Pg boundary was estimated to be too modest to cause an impact winter and alternative studies pointed out that the post-impact sulfur release was a more significant driver behind the prolonged K-Pg impact winter, given the fact that the impact-generated sulfur-bearing gas would have resided in the stratosphere for a period of decades in the form of sulfate particles [Pope et al. 1994; Pierazzo et al. 2003; Toon et al. 2016]. Previous studies reported a longer cessation of solar irradiation as a result of stratospheric sulfate particles relative to the effect of dust particles [Artemieva et al. 2017; Brugger et al. 2017]. Impact-generated soot particles, created by huge forest fires, could also have played a dominant role in the global blockage of solar irradiance and the prolonged post-impact cooling, as fine soot is a strong absorber of the sunlight [Kring and Durda, 2002]. Soot and charcoal remain, found in the K-Pg boundary intervals around the world suggest widespread wildfires in the aftermath of the Chicxulub impact. These wildfires were likely formed proximally during the first 'fireball stage' and potentially also elsewhere on the globe due to the thermal radiation from the atmospheric re-entry of hypervelocity ejecta. In recent studies as the wildfire intensity and magnitude soot production were actively debated [Belcher et al. 2009], the soot production was exclusively linked to the burning of oil-rich shales from the Chicxulub area, as strengthened by the discovery of hydrocarbon combustion products at multiple K-Pg boundaries, such as carbon cenospheres and polycyclic aromatic hydrocarbons [Kaiho et al. 2016]. However, limited knowledge of the extent of organic-rich strata in the Yucatán target stratigraphy makes this assumption difficult to test and a combination of both wildfire and target-rock driven soot emissions cannot be ruled out.

The silicate dust represents another type of fine-grained ejecta, which remains a poorly understood group mainly because of poorly constrained particle sizes. This group is clearly finer than other silicate ejecta, such as coarse glassy impact spherules (i.e., microtektites; with diameters ranging from ~300 µm to 2 mm) and ejected mineral clasts (e.g., shocked quartz, zircon, feldspar; diameters ranging from ~30–600 µm) that are both associated with ejecta curtain processes (Fig. 6a,b), as well as crystalline impact spherules (i.e., microkrystites with e.g., Ni-rich spinels; diameters ranging from ~100-300 µm), which are linked to condensation out of the vapor-rich impact plume (Fig. 6c,d). Two subgroups of silicate K-Pg dust have been

suggested. The first subgroup consists of material with a median diameter of 0.5 µm and is known as submicron clastic dust [Toon et al. 2016]. However, the amount of this subgroup was estimated to be < $6x10^{16}$ g and was therefore considered less significant to the post-impact climate change [Pope et al. 1994]. The other subgroup represents nanoparticles, potentially iron-rich, with a median diameter of 20 nm [Toon et al. 2016]. Their total mass was estimated to be much larger at $2x10^{18}$ g and recent climate model results using ballistic ejection of this subgroup led to an atmospheric removal within nearly two years after impact [Tabor et al. 2020].

To shed light on the K-Pg dust conundrum, we include in this study new and high-resolution sedimentological constraints from an expanded and well-preserved K-Pg sequence from the US Western Interior (Tanis, North Dakota; Fig. 6d; Fig. 7). In contrast to other intermediate or distal K-Pg boundary sites, in which the K-Pg clay interval is often less than 1 cm thick and different types of impact ejecta are often mixed, the unique Tanis K-Pg record is expanded and allows for sub-selection of specific timeframes during the Chicxulub impact ejecta deposition. The ~1.3 m thick ejecta-bearing sediment package, which was emplaced by a Chicxulub impact-generated seiche, was deposited exclusively during the period of coarse ejecta accretion, likely corresponding to < 2 hours post-impact. Shocked quartz has only been found in the un-reworked K-Pg claystone that conformably overlies the impact spherule-bearing Tanis deposit (Fig. 6b, d). Based on ballistic trajectory simulations, shocked minerals are expected to arrive at Tanis in ~2 hours after impact (Alvarez et al. 1995), corroborating the temporal control. A positive iridium anomaly exists in this K-Pg claystone (3.8 ppb), compatible with other globally distributed K-Pg localities (Goderis et al. 2021). We select the uppermost part of the K-Pg claystone interval, just below the Paleogene lignite, to be representative of the final atmospheric settling of the fine silicate dust (Fig. 6d). Laser-diffraction grain-size analysis is performed on the different strata at the Tanis K-Pg site to quantify the particle size distributions. The uppermost K-Pg claystone interval represents a distinct, uniform, and very fine distribution with a volume-based median grain-size of 2.88 µm (Fig. 7a), and after converting to a number-density spectrum; this size distribution data is used here as an input parameter to simulate the silicate dust scenario.

Previous atmospheric modeling studies investigating the radiative effect of the silicate dust following the Chicxulub impact event [Toon et al. 2016] have used either nanometric sized particles or coarse impact spherule data as the bulk fraction of the silicate dust injection, which are estimated to be both in the order of 2 x 10^{18} g. The grain-sizes between ~1-10 µm measured at the Tanis K-Pg site result in significantly slower deposition than those used in previous paleoclimate studies (Fig. 2b). The previously used nanometric sized particles (median diameter of 20 nm) or coarse impact spherules (median diameter of 250 µm) have faster deposition velocities by a factor of ~4 or at least 100, respectively. Here, we incorporate this new sedimentological data in our general circulation model (GCM), which makes use of the latest Cretaceous paleogeographic reconstructions (Fig. 1a) and the latest insights on the moment of impact, which is suggested to be the boreal spring season based on recent data from the Tanis K-Pg site [During et al. 2022]. In our paleoclimate GCM simulations, we injected into the atmosphere the same amount of silicate dust (2 x 10^{18} g), fine soot (2,08 x 10^{16} g**[18]**, using a median diameter of 0.22 µm), and sulfur (3,25 x 10^{17} g of sulfur, equivalent to 6,5 x 10^{17} g of SO_2) as used in recent K-Pg modeling studies, to be able to directly compare the simulation results from our new dust model with previous works [Artemieva et al. 2017; Tabor

et al. 2020; Toon et al. 2016]. Using these input parameters, we model the individual scenarios for silicate dust, soot, and sulfur, accompanied by a combined scenario using all fine-grained ejecta input, to carefully document the short-term global environmental consequences of the Chicxulub impact with a focus on changes in the photosynthetic active radiation.

Our paleoclimate simulations [Senel et al., submitted] show a global-average seasonal maxima of 19°C before the impact event, in line with proxy-based latest Cretaceous temperature reconstructions [Niezgodzki et al. 2017]. The K-Pg impact winter catastrophically disrupted this greenhouse climate, leading to plummeting temperatures in both the marine and especially the terrestrial realm. The global-average surface temperature dropped by as much as 25˚C (Fig. 8a). With varying magnitude and timescales, each fine-grained ejecta type results in a prolonged global cooling in the initial aftermath of impact. The sulfur scenario causes the lowest surface temperatures, i.e., with a global average of -5 ˚C, followed by the silicate dust scenario, i.e., with a global average of ~5 ˚C. Our simulation results indicate that both sulfur and silicate dust have a prominent influence on the surface thermal forcing, leading to a prolonged impact winter up to ~20 years.

The ejecta type and its atmospheric mass determines the magnitude and timescale of the impact winter (Fig. 8b), related to different responses in downward longwave radiation (Fig. 8c) and net shortwave radiation on the surface. The downward longwave radiation, as an indicator of the reflected radiation due to atmospheric particles and clouds, may either diminish or further enhance the surface warming. The sulfur in the atmosphere decreases much faster than dust, in which the global column-integrated mass of sulfur is reduced to about one order of magnitude lower than that of dust at 4 years after impact (Fig. 8b). Considering the radiatively transparent feature of sulfate particles relative to silicate dust particles, the sulfur release is not capable of downward longwave radiation enhancement, reducing by 33% from the pre-impact level in just a few years. On the contrary, the dust-induced downward longwave radiation shows a rapid increase by 81% from the pre-impact level to 380 W/m^2 within a week after impact, decreasing below the pre-impact level in the next ~3 years (Fig. 8c). Following the first 4 years after impact, which is associated with the initial extreme cold (Fig. 8a), our results show that large anomalies in surface net shortwave and longwave radiation fluxes stabilize to pre-impact levels.

The global-average photosynthetic active radiation (PAR) flux in the sunlight spectrum varies seasonally between 80 and 95 W/m^2 in the latest Cretaceous (Fig. 8d). As a consequence of the seasonality, the PAR flux is as high as 160 W/m^2 in the northern hemisphere just before the impact winter. The two-days response (Fig. 9) displays the trace of initial ejecta expansion through the atmosphere, marking a regional PAR deficit on the surface. Given that the dust and sulfur are ejected from the impact target, their traces are initially centralized around the Yucatán area, unlike the global spread of soot released from wildfires. Within a week after impact (Fig. 8d), the planet undergoes a global shut-down in photosynthetic activity in all ejecta scenarios. Consistent with global-average responses (Fig. 8d), the massive dust ejecta indicates the largest influence on the land-ocean photosynthetic activity, leading to an entire PAR suppression for at least ~2.7 years (Fig. 9a). Even 3.2 years after impact, during boreal summer, the photosynthetic activity remains still in partial recovery with a moderate PAR flux of 80 W/m^2, reaching pre-impact values in almost ~5 years (Fig. 8d, Fig. 9a). Following the initial suppression of six months (Fig. 8d), the PAR loss is completely recovered in the sulfur

and soot scenarios over the next ~2 years after impact (Fig. 9b, c). Furthermore, similar to the dust-induced response, the combined scenario indicates a complete PAR suppression for at least ~2.7 years (Fig. 9d), which fully recovers only after ~5 years after impact (Fig. 8d).

In contrast to previous work**,** our paleoclimate simulations revealed that a massive impact-generated dust plume may in large part drive the K-Pg climate and biotic crisis [Senel et al., submitted]. This dust cloud is composed of a large number of climate-active particles with particle sizes primarily in the range of 1-10 µm by volume (Fig. 7a), which would result in an atmospheric residence time that is much longer (> 4 times) compared to nano-sized or coarse particles (Fig. 7b; 8). Among the simulated ejecta types, our results demonstrate a post-impact world where dust represents the largest ejected mass in the initial aftermath of impact (Fig. 8b). The sulfur scenario exhibits the fastest deposition with an atmospheric lifetime of ~7 years. In contrast, both soot and silicate dust resided in the atmosphere considerably longer for at least ~20 years after impact. The combined scenario falls between the sulfur and dust cases with an atmospheric lifetime of ~16 years, implying a plausible condition for the Chicxulub impact (Fig. 8b). The complete recovery from the impact winter took even longer, with pre-impact temperature conditions returning only ~20 years after impact (Fig. 8a). This timescale is consistent with the recent global iridium layer observations [Goderis et al. 2021] from within the Chicxulub impact structure, in which the final atmospheric settling of impactor material in the dust cloud was estimated to be ~20 years.

We find that the global darkness and prolonged loss in the planet's photosynthetic activity occur only in the silicate dust scenario, up to nearly 3 years after impact (Fig. 8d; Fig. 9), implying a sufficiently long timescale to pose severe challenges for both terrestrial and marine habitats. Biotic groups that are not adapted to survive the dark, cold and food-deprived conditions for at least two years, experienced massive extinctions. This matches the paleontological records, which show that fauna and flora that could enter a dormant phase (e.g., through seeds, cysts, hibernation in burrows), and are able to adapt to a generalist lifestyle not dependent on one particular food source (e.g., deposit feeders), generally survive the K-Pg event [Vellekoop et al. 2020]. In addition, our results show that the photosynthetic recovery to the pre-impact levels first occurred in the austral summer season, ~2.7 years after impact. This would imply an earlier recovery of the primary productivity in the Southern Hemisphere, consistent with paleontological evidence suggesting lower extinction rates on the Southern Hemisphere, resulting in geographic heterogeneity in extinction and recovery from the end-Cretaceous catastrophe [Donovan et al. 2016]. However, more high-resolution studies of K-Pg boundary records around the globe are needed to confirm the degree of hemispheric heterogeneity in the post-impact biotic recovery.

In summary: our new results highlight that the photosynthetic shut-down induced by the large volume of dust with grain-sizes between ~1-10 µm, together with additional effects of sulfur and soot, presented in various other models, would have led to a disastrous collapse of primary productivity in land and ocean realms, steering the global mass extinction at the K-Pg boundary.

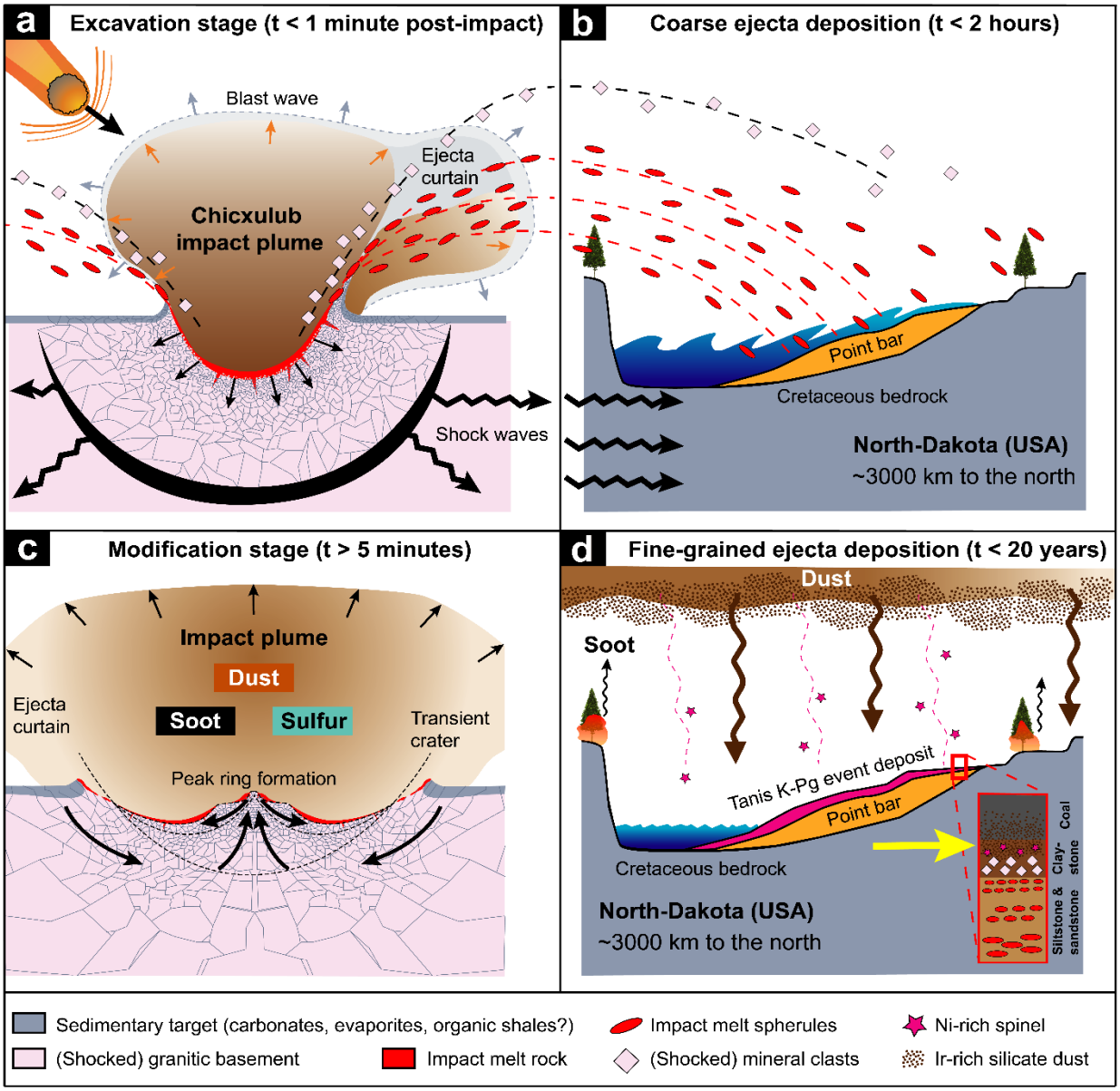

Figure 6. Conceptual model of the Chicxulub plume showing the stages of production, transport, and deposition of coarse and fine-grained impact-generated ejecta (model not to scale**. a)** The excavation stage displays a 45° impact of a 10-15 km sized bolide from the NE [Collins et al. 2020]. The target rocks are displaced to form a transient cavity with an uplifted rim and are ejected within an impact plume and curtain. Melt spherules and shocked minerals deriving from the granitic basement are expelled. **b)** At the terrestrial Tanis K-Pg site in North Dakota (USA), ~3000 km towards the north, the rapidly moving impact-induced shock waves induce shaking of a shallow sea causing a seiche-inundation event. Meanwhile, the glassy impact melt spherules are – largely ballistically – emplaced in the event deposit, followed by the arrival of the shocked mineral clasts (mainly quartz, zircon), that are ballistically expelled at a higher angle than the melt spherules, constraining the time of deposition at ~2 hours [Alvarez et al. 1995]. **c)** At the impact site, the cavity rim collapses whereas rocks in the central area are first uplifted and then subside downwards and outwards to form a peak ring. Meanwhile, the impact plume with fine-grained ejecta (silicate dust, soot, and sulfate particles from S-bearing gases) is growing and rising to the stratosphere and distributes material around the globe. **d)** At the Tanis K-Pg site, after the rapid emplacement of the coarse-grained ejecta bearing event deposit, atmospheric settling is taking over with Ni-rich spinel, soot particles, and a large fraction of silicate dust. The panel shows a schematic stratigraphy of a silt-to sandstone interval with glassy impact spherules, followed by a claystone interval with shocked minerals, Ni-rich spinels, and fine dust rich in iridium, overlain by a coal**.** This study focuses on the claystone interval just below the Paleogene coal unit, as this layer is indicative for the settling of very fine-grained impact-generated silicate dust in the first years after the Chicxulub impact, as illustrated by the yellow arrow. [Senel et al., submitted].

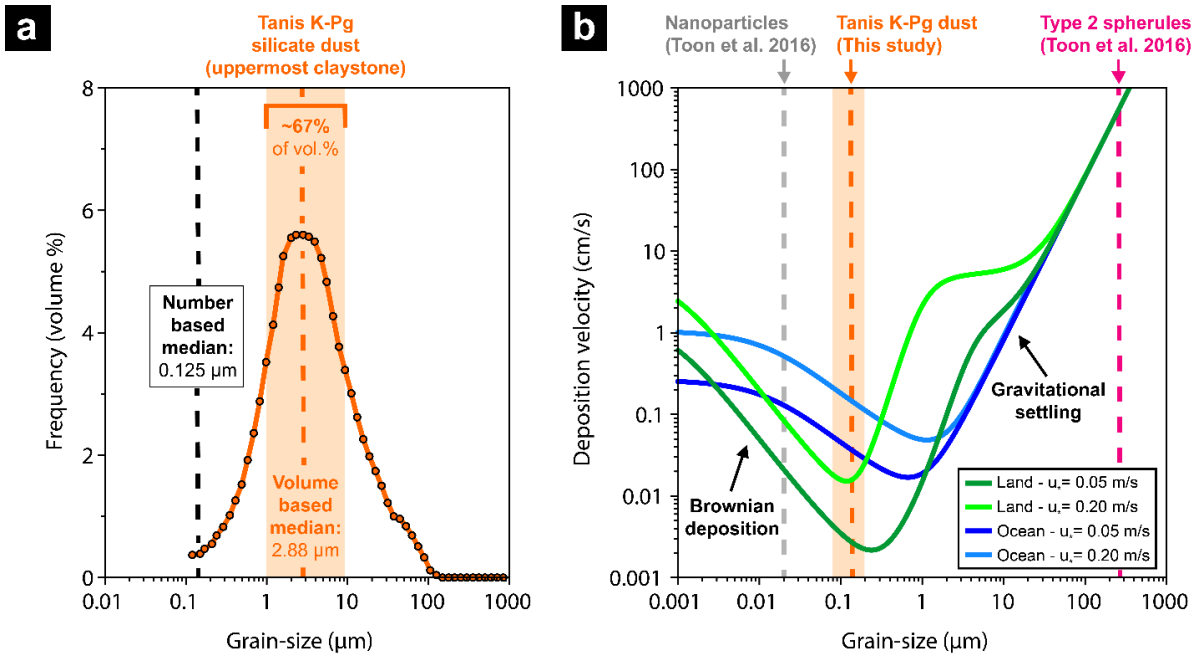

Figure 7. K-Pg boundary grain-size data in relation to atmospheric settling processes. **a)** Laser-diffraction grain-size distribution curve of the silicate lithogenic fraction for the uppermost K-Pg boundary claystone level from the Tanis site, just below the Paleocene lignite. The orange curve displays the volume-based grain-size distribution, the black dashed line highlights the median grain-size value after a conversion into a number-density spectrum. **b)** Phase diagram shows grain-size versus the variation of dry deposition velocity over land (green solid curves) and ocean (blue solid curves) for two different friction velocity values, u_*, indicating the intensity of surface wind shear. The largest fraction of ejected dust used in previous modeling studies (Tabor et al. 2020) is either nanometric in size (median of 0.02 µm; see gray dashed line), following a fast Brownian deposition, or close to millimetric in size (median of 250 µm; see purple dashed line) in terms of type 2 spherules (i.e., microkrystites), following a fast gravitational settling. This contrasts the silicate dust fraction measured at the Tanis K-Pg site (number-based median of 0.125 µm with two thirds of the particles by number-density falling in the range of ~0.08 - 0.2 µm; see orange dashed line and bar), implying considerably slower deposition out of the atmosphere. (Senel et al., submitted).

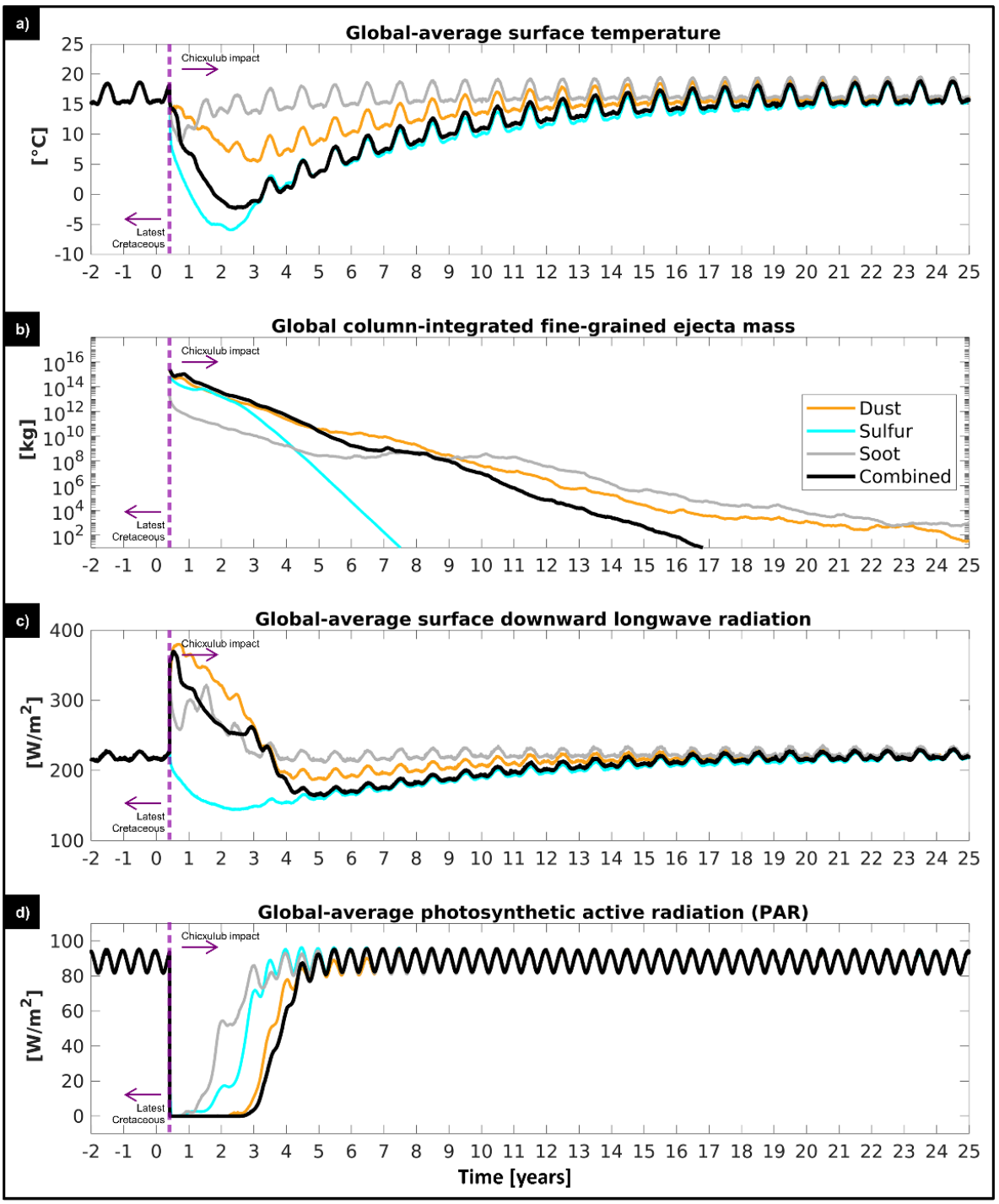

Figure 8. Temporal evolution of the Chicxulub impact-generated global climatic responses. The time evolution is shown from 2 years of the latest Cretaceous towards 25 years of post-impact conditions, for the individual silicate dust, sulfur, soot, and combined scenarios. a) Global-average surface temperature. b) Global column-integrated fine-grained ejecta mass. c) Global-average surface downward longwave radiation flux. d) Global-average photosynthetic active radiation (PAR) flux. The combined scenario refers to the simulation of each fine-grained ejecta type (sulfur, soot, and silicate dust) that concurrently is released to the atmosphere. Here in x-axis, the year of 0 refers to the start of the year where the impact event occurs. The solid purple dashed line denotes the moment of Chicxulub impact, i.e., during the boreal spring season. [Senel et al., submitted]

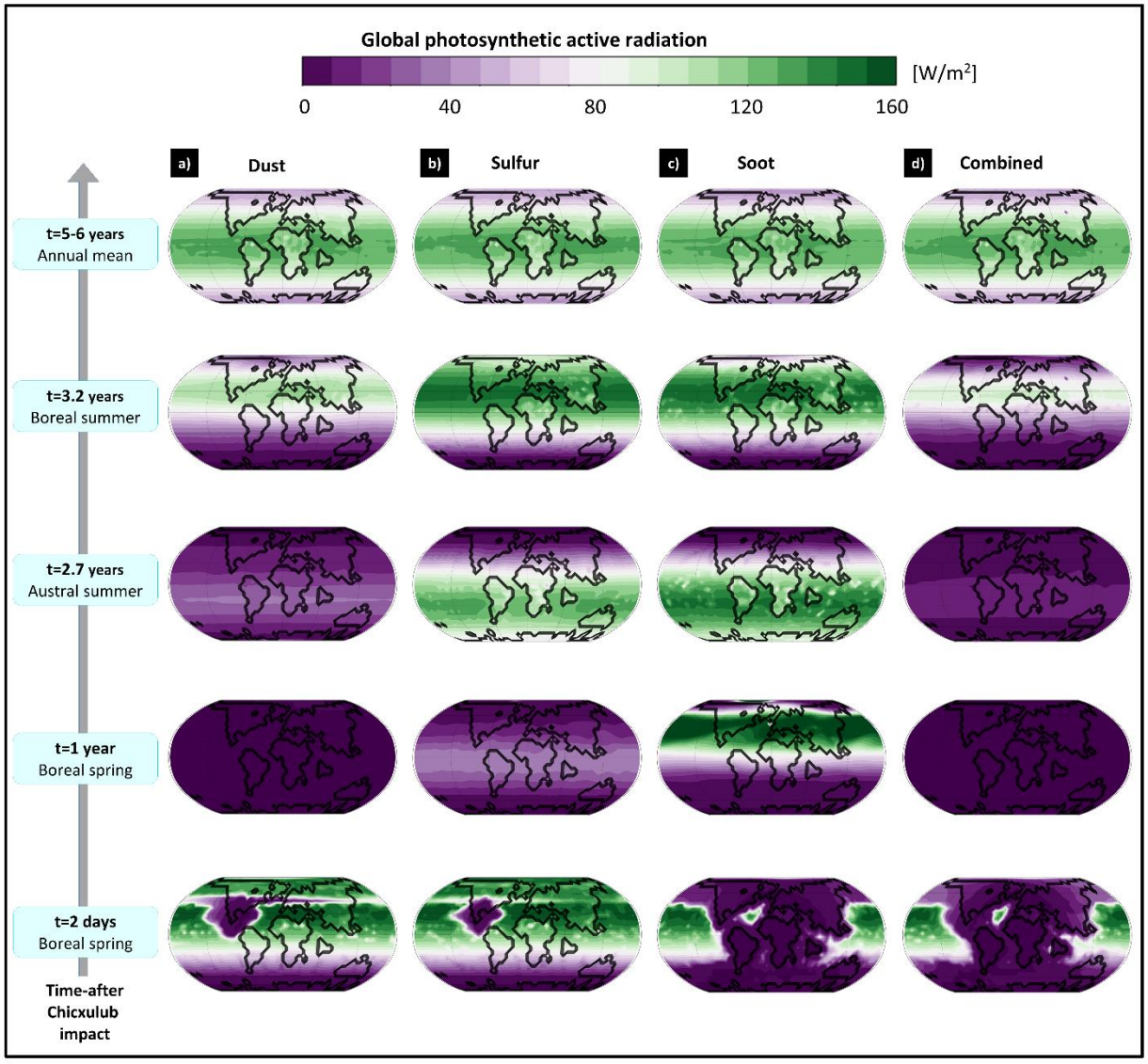

Figure 9. Temporal evolution of photosynthetic active radiation (PAR) flux reconstructions after the Chicxulub impact. Land and ocean PAR flux from 2 days (instantaneous) towards 5 to 6 years (annual mean) in the aftermath of the Chicxulub impact for a) silicate dust; b) sulfur; c) soot; and d) combined scenarios, displayed on a latest Cretaceous paleogeographic map (Extended Data Fig. 1a). The range of the green and purple colorbar represents the photosynthetically high and low radiative flux. Note that the PAR flux colorbar varies between 0-160 W/m^2 for all time snapshots, except for t=1 year (boreal spring) that ranges between 0-30 W/m^2 for the sake of visibility in differences between ejecta types. [Senel et al., submitted]

3.3) Third objective: test the link between the Chicxulub crater formation and the Deccan eruption peak at the K-Pg – *WORK PACKAGE 3* –

3.3.1) Introduction

This work-package included the study of the ICDP Koyna core stored in India at the Borehole Geophysics Research Laboratory in Karad. The ICDP Koyna project recovered a full core through the central part of the Deccan trap all the way to the Archean basement (1500 http://www.icdp-online.org/projects/world/asia/koyna/details/).

This WP could not be carried out within the project period because of Covid and the impossibility to carry out field work in India in 2020 of in 2021. We received some samples

of these cores from our Indian colleagues but were not able to locate the K-Pg boundary based on the information and material received. Clearly, field work and macroscopic examination of the Koyna cores are imperative to accomplish the goals described in this WP, which was to check if as postulated the Chicxulub impact triggered a major output of Deccan volcanism. We remain in contact with Dr. Sukanta Roy, head of the Borehole Geophysical Laboratory in Karad, India where the Koyna core is currently curated in order to sample this material using AMGC own funding in 2023 or 2024.

Instead, this WP 3 was replaced by a careful sedimentological and geochemical study of US Western Interior K-Pg boundary sites to refine our understanding of ejecta arrival time, as these samples were available to us without having to travel. The main results of this approach obtained at the Tanis K-Pg site in North Dakota have been described in detail and used in WP2 to constrain the dust model. Below is the description of another high-resolution profile across the boundary carried out at Starkville-South in the Raton basin in Southern Colorado.

3.3.2. Material & methods

We selected a sample that was collected in 2005 from the K-Pg boundary site of Starkville-South from the Raton Basin in southern Colorado (USA) (AMGC collection), which is characterized by highly elevated iridium concentrations between 16-56 ppb. This sample was stabilized with plaster of Paris and epoxy, and was subsequently cut and polished, preserving a continuous microstratigraphy of claystone and lignite [8]. The resin slab (3 x 4 cm; Fig. 10) was measured with non-destructive element mapping and spot analyses using an M4 Tornado benchtop µXRF scanner (Bruker nano GmbH, Berlin, Germany) equipped with a Rh tube as X-ray source and two XFlash 430 Silicon Drift detectors. The µXRF mapping was carried out under near-vacuum conditions (20 mbar), using both detectors at maximized X-ray power (50 kV, 600 µA) and with a pixel size resolution of 10 µm and integration time of 100 ms per pixel.

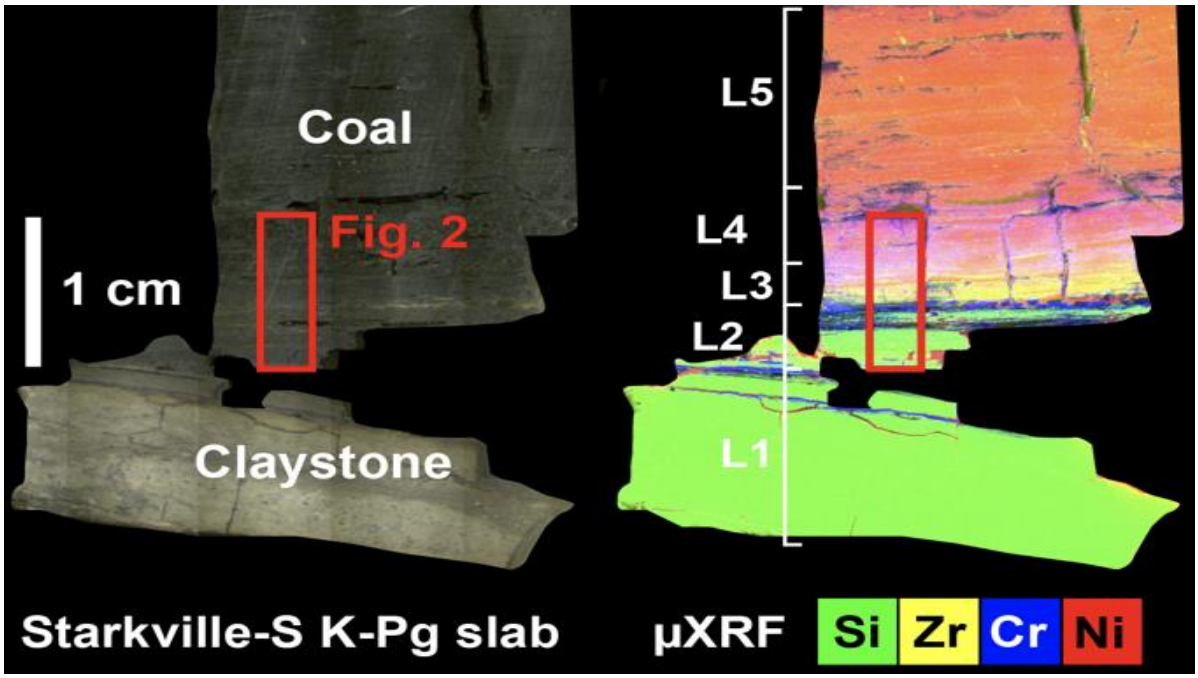

Figure 10. The Starkville-South K-Pg boundary resin slab with an µXRF multi-element map showing the distributions of Si, Zr, Cr, and Ni, which were used to identify five distinct layers (L1-L5). The red rectangle indicates the stratigraphic position of the averaged linescan data displayed in Fig. 11.

In addition, 20 nanomilled powders of certified geological reference materials (ranging from felsic and mafic igneous rocks to carbonates) were analyzed by µXRF spot analyses (average RSD < 15%) to produce a multi-standard, matrix-matched calibration. The quantification was done by combining the fundamental parameters algorithm integrated in the M4 µXRF software with these reference samples, resulting in the quantification of 25 major and trace elements (R2 values > 0.99 for Na, Mg, Al, Si, S, Cl, K, Ca, Ti, V, Cr, Mn, Fe, Co, Ni, Cu, Zn, Ga, As, Rb, Sr, Y, Zr, Nb, and Pb), Subareas within the µXRF maps were extracted using the linescan function in the M4 software to produce chemical profiles of the K-Pg boundary interval (Fig. 11).

3.3.3. Results and discussion

The µXRF mapping of the Starkville-S slab detected 27 elements. Based on the distribution of Si, Zr, Cr and Ni, we subdivided the K-Pg boundary interval into five distinct layers (Fig. 10; 11). The lowermost stratum (L1: >1 cm thick) represents a relatively homogeneous claystone rich in Si and Al (Fig. 10). The overlying clay layer (L2: ~4 mm thick) is comparable in bulk geochemistry but has clear hotspots enriched in both Si and Zr (Fig. 11) The third layer (L3:~3 mm thick) is a transition from claystone to lignite and is characterized by low Si values and a bulge of high Zr- concentrations (up to 1 wt%) and elevated values for Cr and Ni (Fig. 11). The fourth layer (L4: ~5 mm thick) is a lignite with decreasing values for Zr, but it still yields elevated Cr content and the highest values for Ni (Fig. 2). The upper layer (L5: >1 cm thick) is a homogeneous lignite low in Si, Zr, Cr and Ni content (Fig. 11).

The Starkville K-Pg impact ejecta sequence started with the deposition of glassy impact spherules (microtektites) derived from a turbulent Chicxulub ejecta curtain that arrived at this location approximately 15 minutes after impact Artemieva and Morgan (2020). These spherules subsequently altered and now form the thick kaolinitic boundary claystone (L1). L2 is characterized by the presence of (shocked) quartz and zircons, which were likely ballistically expelled under a higher angle (>65°) and therefore deposited in a slightly later stage on top of the layer with the impact spherules Alvarez et al. 1995. This layer is known as the 'fireball layer', and U/Pb ages of highly shocked zircons from this layer in the Raton Basin have revealed a link to the ~66 Myr old Chicxulub impact structure. L3 is dominated by the highest Zr concentrations, which is interpreted as being related to a pulverized fraction of the felsic crystalline basement incorporated within the impact plume. Geochemical analyses of granitoids from the recent IODP-ICDP Expedition 364 drilling within the Chicxulub peak ring have shown average Zr values of ~100 ppm (See WP1). The enriched Zr values in L3 are most probably related to the refractory behavior of Zr within the impact plume. L4 displays a bulge of high Ni values (up to 1000 ppm), which hint towards a dominance for fine dust enriched in iridium and other PGEs (see WP1). Peaks of Ni and Cr (both up to 2 wt% in hotspots) suggest the presence of microkrystites with Ni-Cr-rich and Mg-poor spinels. This would imply that the deposition of L4 is steered by condensation processes and atmospheric settling of ultrafine impactor dust within a paludal environment. Previous work has estimated that this process could take up to ~20 years after impact (see WP 1 & Goderis et al. 2021).

In summary: High-resolution µXRF mapping of the K-Pg boundary sequence at Starkville has revealed a more complex microstratigraphy than the 'dual-layer' succession described in literature. Detailed petrographic analysis is aimed to confirm and extend our observations and provide new input parameters for atmospheric climate and ejecta models (see WP2).

This will shed light on the timing and mechanisms of impact ejecta processes for Chicxulub and other impact events in the Solar System.

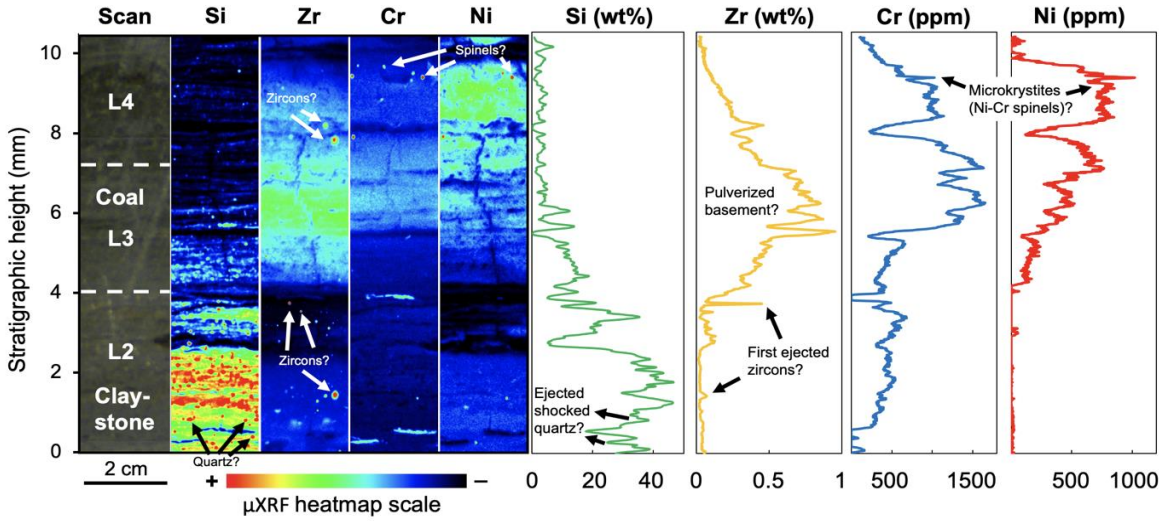

Figure 11. Zoom-in of the Starkville-South K-Pg boundary slab showing semi-quantitative µXRF heatmaps of Si, Zr, Cr, and Ni. The arrows indicate mineral phases linked to different types of impact ejecta. The profiles on the right are extracted from the µXRF maps and show absolute concentrations of Si, Zr, Cr and Ni, averaged per stratigraphic height and quantified using a new calibration.

3.4) Fourth objective: impact on latest Cretaceous faunas– *Work Package 4*

3.4.1) Introduction

We further explored the impacts of Deccan volcanism and Chicxulub impact in the marine realm, in particular on iconic marine macrofauna like ammonoids and nautilids (Class Cephalopoda, Phylum Mollusca). The differential evolutionary success of both groups of externally shelled cephalopods has puzzled scientists for many decades, and still puzzles them today. In the past 20 years, the ammonoid extinction received a lot of attention and many important advancements in the understanding of this extinction have been generated, while at the same time, the 'nautilid side of the story' has never been thoroughly investigated and currently remains one of the last unexplored issues of the K-Pg boundary biotic crisis. We also further expanded to other mollusks like gastropods and bivalves from K-Pg boundary sites close to home (type Maastrichtian area, The Netherlands, Belgium), as well as to crustacean faunas further away (Tunisia, northern Africa).

3.4.2) Ammonites during main phase of Deccan volcanism.

For the ammonoids, there is overwhelming evidence that their final extinction is abrupt and correlates well in time with the environmental perturbations in the immediate aftermath of the Chicxulub impact, but the possibility of Deccan volcanism altering their distribution and diversity in the hundreds of thousands of years prior to Chicxulub impact is still poorly investigated.

Through collaboration with Prof. Johan Vellekoop (KULeuven), Prof. em. Jan Smit (VU, The Netherlands), Dr. Sanem Açikalin (Newcastle University, UK), Uygar Karabeyoglu and Prof. Ismail Omer Yilmaz (METU, Turkey), we discovered 4 new ammonoid bearing K-Pg boundary sites in the Sarkaya region, central Anatolia, Turkey. Each of these sites is biostratigraphically complete, has a well-preserved Chicxulub ejecta layer and has ammonoids up to the highest

1 m of the section, in some even up to the highest 1 cm. The four sites, Okçular, Goynuk West and Dedeler in the Mudurnu-Göynük Basin and Cayraz in the Haymana Basin, surprisingly allow to document two totally different faunas only 180 km apart. One is characterized by the dominance of scaphitids (Ancyloceratina), the other by the complete absence of scaphitids. No ammonites are recorded from the basalmost Paleocene, so that the Turkish sites again favor a relationship between their extinction and the Chicxulub impact.

Not unimportantly, these 4 sites, and in particular the one of Cayraz, turned out to be key stone in the furthering of our understanding of the distribution, both geographically and environmentally, of terminal Maastrichtian ammonites. These 4 sites were added to the other 29 sites previously inventoried with ammonites present within the topmost 0.5 myr of the Maastrichtian. This time interval correlates to the main phase of Deccan volcanism. The new sites fill in yet another blind spot on the world distribution map, and one relatively close to Deccan volcanism (Fig. 12).

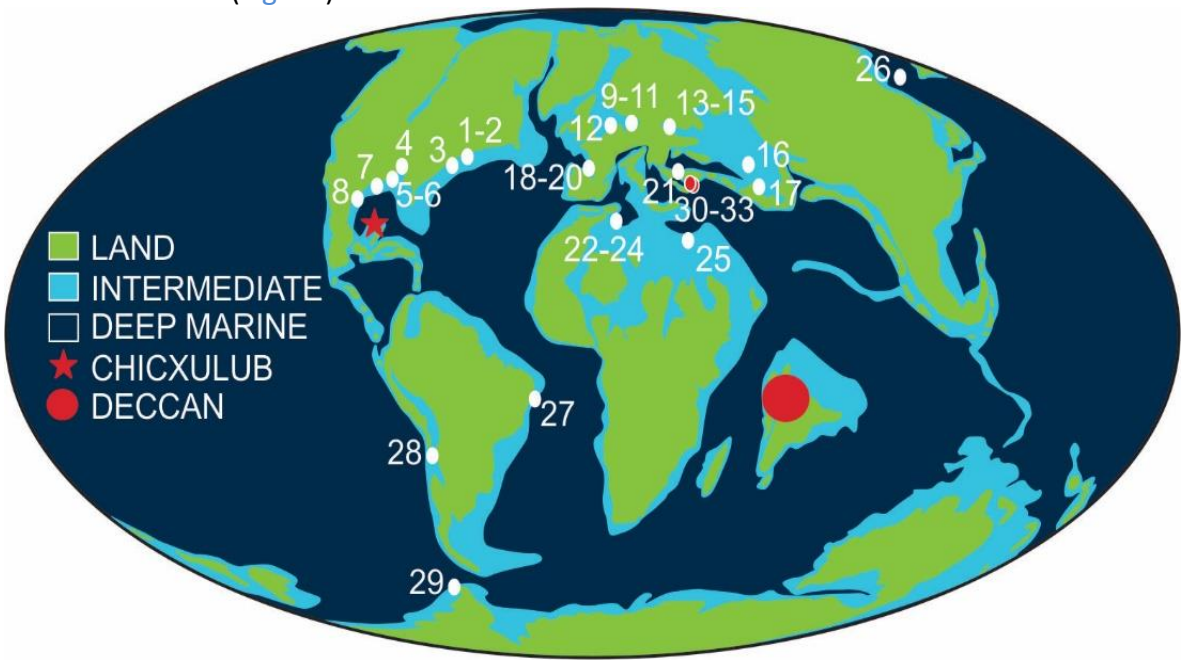

Figure 12. Updated map of all known sites with ammonites from within the last 0.5 myr of the Cretaceous. The four new Turkish sites are numbered 30 to 33. The same numbering is used in the figures below. (Goolaerts et al unpublished)

When we added paleodepth and sampling intensity for all 33 sites to the table of generic occurrences (Fig. 13), a distinctive twofold clustering became apparent between those sites where scaphitids and baculitids are present and those where these are absent. Furthermore, the first cluster (scaphitid+baculitids present) can be further divided into four smaller clusters, three of them based on the occurring scaphitid genus, plus a fourth from which only Baculitidae are listed. The first three all locate in the northern hemisphere, and because northern American sites only preserve *Discoscaphites*, Eurasian sites only *Hoploscaphites* and north African sites only *Indoscaphites*, a clear paleogeographic clustering can also be observed. On top, in all sites of the first 'mega'cluster, scaphitids and baculitids take at least 60 and sometimes up to 100% of collected specimens into account. In the second cluster, which is spread across both hemispheres, the faunal composition is completely different and much more evenly spread across the occurring genera. Also, in that cluster, with the exception of the supposedly facies independent 'paperclip shaped' *Diplomoceras*, no

representatives of the Ancyloceratina (=heteromorph ammonites) are known, and Lytoceratina and Ammonitina become the most abundant faunal elements.
Paleodepth clearly seems the most important character responsible for this clustering, next to paleogeography. Our results also show that each cluster has a different (maximal) generic diversity, with the highest diversity being found at the deeper water sites of the first cluster, most probably because here the 'two realms' meet (Figs. 14, 15). Our results have major implications for those studying ammonoid biostratigraphy, diversity and extinction, and need to be extrapolated to earlier parts of the Maastrichtian. Next to paleodepth and paleogeography, also collecting intensity is of major importance when a site's generic diversity is assessed (Fig. 16). The shallow water type Maastrichtian still has a very high generic diversity but resulting from >150 years of intensive collecting. For ¼ of the sites, less than 10 specimens are recorded, and for ¾ less than 100, meaning that for many sites, generic diversity is currently heavily underestimated. This can be revealed by pooling all genera of a given cluster together and comparing it to the number of genera per site in the same cluster (Fig. 16).

				GROUP 1: SCAPHITIDAE AND BACULITIDAE DOMINANT																								GROUP 2: SCAPH + BAC ABSENT								
				Discoscaphites realm								*Hoploscaphites* realm												*Indoscaphites* r.				Tethyan Seaway					Other		
SUBORD	FAMILY		Site and site number	AR	ML	AM	AN	AR	GS	GT	GC	GB	MA	PN	PM	PL	KA	TR	DS	DK	DD	OK	GO	DE	TK	TE	TG	EG	BZ	BH	BB	BU	CA	SA	AN	BR
		n°	Genus	28	8	1	2	3	4	5	6	7	12	13	14	15	16	17	9	10	11	31	32	33	22	23	24	25	18	19	20	21	30	26	29	27
PHYL	PHYL	1	*Phylloceras*																1		1				1				1	1	1		1	1		
		2	*Phyllopachyceras*																						1				1	1	1					
LYTOCERATINA	GAUDRY	3	*Gaudryceras*									1																	1				*	1		
		4	*Anagaudryceras*																						1				1	1	1	1	*	1	1	
		5	*Vertebrites*																													1	*			
		6	*Zelandites*																						1	1			1					1	1	
	TETRA	7	*Tetragonites*																						1	1							*			
		8	*Saghalinites*																1		1				1						1					
		9	*Pseudophyllites*																						1	1	1				1	1	*		1	
AMMONITINA	DESMO	10	*Desmophyllites*																										1							
		11	*Hauericeras*																						1	1	1									
		12	*Kitchinites*																																1	
	KOSSMA	13	*Pseudokossmaticeras*																												1					
		14	*B. (Brahmaites)*										1												1	1	1			1			1			
		15	*Grossouvrites*																																1	
		16	*Maorites*																																1	
	PACHY	17	*P. (Pachydiscus)*									1	1	1											1	1	1		1	1	1	1	1	1	1	1
		18	*P. (Neodesmoceras)*			1			1																1	1	1							1		
		19	*Menuites*										1	1					1		1				1	1	1		1	1	1	1	1			
	S.	20	*Sphenodiscus*		1	1	1		1	1	1		1	1																						
ANCYLOCERATINA	N.	21	*Nostoceras*										1																							
	DIPLO	22	*Glyptoxoceras*									1	1																							
		23	*Diplomoceras*										1						1		1				1	1	1			1	1			1	1	1
		24	*Phylloptychoceras*										1						1						1	1	1									
	BAC	25	*Baculites*		1				1	1	1		1	1	1	1	1	1	1	1	1				1	1	1	1								
		26	*Eubaculites*	1		1	1	1	1	1	1	1	1																							
		27	*Fresvillia*																						1	1	1									
	SCAPH	28	*Indoscaphites*																						1	1	1	1								
		29	*Hoploscaphites*										1	1	1	1	1	1	1	1	1	1	1	1												
		30	*Acanthoscaphites*										1																							
		31	*Discoscaphites*			1	1	1	1	1	1	1																								
			N genera/site	1	2	4	3	2	5	4	4	5	12	5	2	2	2	2	7	2	6	1	1	1	17	13	11	2	8	7	9	5	6	7	8	2
			collected specimens	a	a	b?	b?	b?	b?	b?	b?	c	d	d	a?	a?	b	b	d	a?	b?	a	a	a	d	c	c	b	b?	b?	b?	b	b	b	c	a
		Environm.	very shallow	x	x	x	x	x	x	x	x	x	x	x	?	?	?																			
			shallow					?				?			?	?	?																			
			intermediate-deep														?	x	x	?	x	x	x	x	x	x	x	x						?	x	?
			deep-very deep															?								?			x	x	x	x	x	x	?	

Figure 13. Table with generic occurrences of ammonites with sites documenting the last 0.5 myr of the Cretaceous. Sites are clustered together based on similarities of the fauna. Remark a large dissimilarity between the shallow water sites which have nearly always scaphitids and baculitids present and those of the deeper (=open marine) settings in which scaphitids and baculitids are completely absent. The same numbering is used as in Fig. 12. (Goolaerts et al unpublished)

With these data on hand, added with the actual collecting numbers of three Tunisian sites (EK, GH, KS) and Cayraz (CA), it was attempted to create a paleoecological model for ammonites during Deccan volcanism (Fig. 17) explaining the observed differences between

the ammonite faunas of the different sites and clusters. The model of Fig. 4.5 is plotted against a hypothetical depth gradient and allows to explain the composition of the fauna of nearly all 33 sites. A first report on the outcomes was presented at the 2018 Annual Meeting of the Geological Society of America in Indianapolis, and a more mathematical approach to the clustering was tested with Jérémie Bardin (UMPC, Paris) in July 2019 but with yet unsatisfying results.

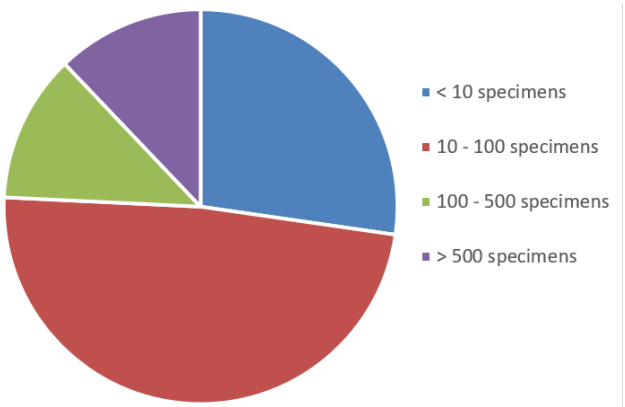

Figure 14. Pie diagram showing the percentage of sites <10, 10-100, 100-500, >500 specimens. Of these 33 sites, more than ¼ have less than 10 specimens recorded, and ¾ less than 100, which means that the alpha diversity at a given site will be most probably (<10 specimens) to probably (10-100 specimens) underestimated. And even at those sites from which more than 500 specimens are recorded, one or several species are only recorded by one specimen. (Goolaerts et al unpublished)

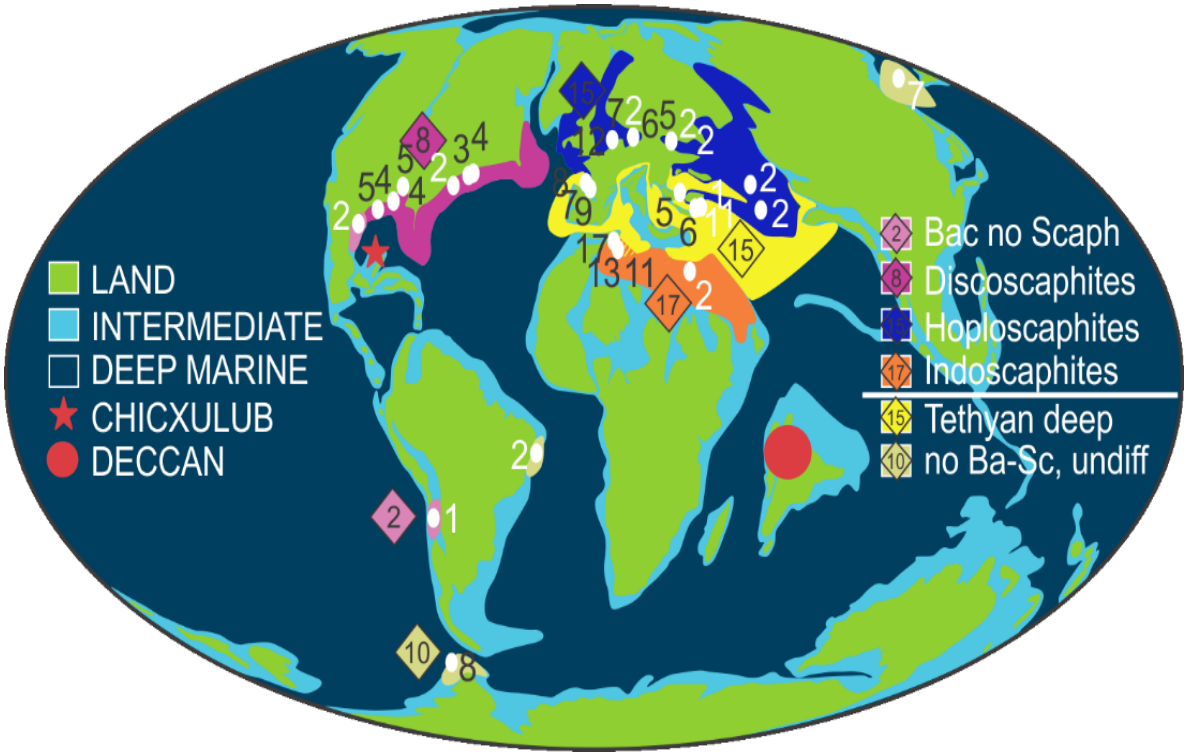

Figure 15. The same map of figure 12 but with the generic diversity per site in white (very low number of specimens yet recorded from this site) or black (higher number of specimens recorded), and in squares the combined generic diversity for one of the clusters. (Goolaerts et al unpublished)

The identification the possible effects of Deccan volcanism on ammonoid faunas is hampered by the low number of sites from which both a large number of collected specimens (less than

¼ of the 33 sites, Fig. 14) and bed-by-bed collecting data are known. In some of them, like the Tunisian sections, a diversity increases rather than a diversity decrease seems to correlate with the timing of the onset of the main phase of Deccan volcanism (Fig. 17). In the type Maastrichtian area, some of the new arrivals may correlate with a warming pulse possible related to Deccan volcanism, but much more analysis is needed to establish a clear causal relationship.

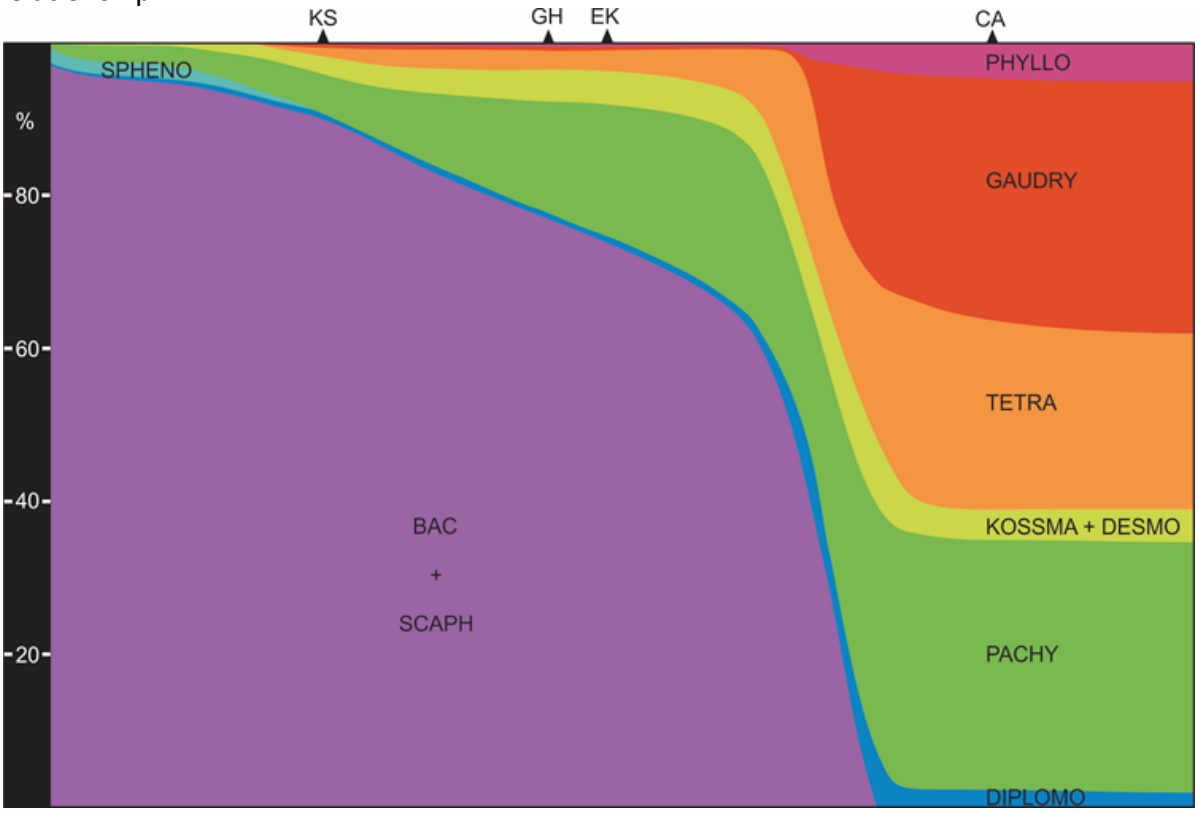

Figure 16. Paleoecological model for ammonite faunas during the main phase of Deccan volcanism along a theoretical depth transect from shallow water (left) to open marine settings (right) based on the occurrences and their dominance of the 33 sites. [Spheno: *Sphenodiscus*; Bac: Baculitids; Scaph: Scaphitids; Phyllo: Phylloceratins, Gaudry: Gaudryceratids, Tetra: Tetragonitids; Kossma: Kossmaticeratids; Desmo: Desmoceratids; Pachy: Pachydiscids; Diplomo: *Diplomoceras*]. (Goolaerts et al unpublished)

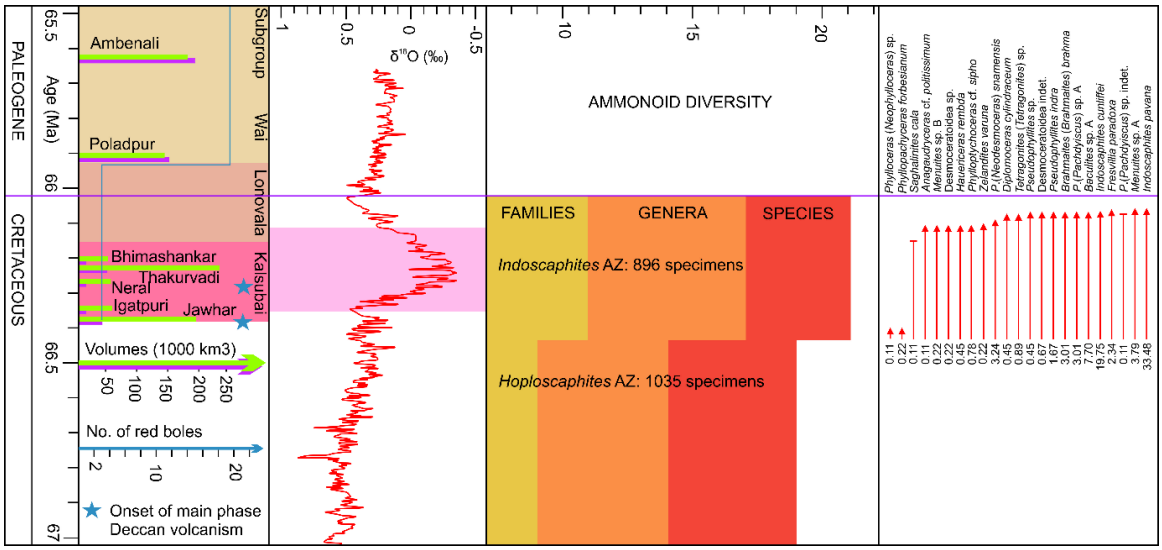

Figure 17. Number of families, genera and species of the two highest ammonite faunas from Tunisia plotted next to timing of Deccan volcanism. A diversity increase almost coincides with the onset of the main phase of Deccan and Deccan warming. (Goolaerts et al unpublished)

3.4.3) Heteromorph ammonites surviving Chicxulub impact

Ammonites are also reported from beds above the K-Pg boundary. However, most of the in literature reported records of ammonites found above the K-Pg boundary relate to reworked Cretaceous (or older) specimens in Paleocene (or younger) beds, or to erroneous placement of the K-Pg boundary level. From only one site possible victims of the Chicxulub impact are known. At Tanis, North Dakota, some shells of the non-heteromorph *Sphenodiscus* are reported in literature to occur in the seiche beds related to the impact, but the data of the publication, it cannot be assessed if these are true Chicxulub impact victims or somewhat older shells that were ripped up from the seafloor or shallowly buried sediments and redeposited within the seiche beds (DePlama et al. 2019).

The only possible true temporary K-Pg boundary survivors are found in Denmark, the type Maastrichtian area (The Netherlands, Belgium) and New Jersey. In Denmark, ammonites from the lowermost Danian Cerithium Limestone were known for more than a century but were routinely considered as reworked material, until early Danian age infillings of shells were reported, favouring the true early Danian survivor hypothesis. All reported survivors are heteromorphs; the scaphitid *Hopscaphites constrictus johnjagti* and the baculitid *Baculites vertebralis*. Age dating of the Cerithium Limestone place these records in-between 40 to max. 500 kyrs after the K-Pg boundary.

In the type Maastrichtian area, ammonites are still found up to 2 m above the K-Pg boundary level that situates in-between the IVf-6 and IV-f7 units of the Meerssen Member of the Maastricht Formation (Vellekoop et al. 2020). Like in Denmark, the fauna exists exclusively of heteromorphs; baculitids *Eubaculites latecarinatus* and *Baculites* spp. and scaphitid *Holopscaphites constrictus johnjagti*. By the preservation of their delicate apertures, in combination with a taphonomical analysis of all other collected fauna and a study of the faunal composition, the possibility of reworking from older deposits can be excluded and these occurrences can be interpreted as true temporary survivors. In contrast to Denmark, the ammonites are from within the first hundreds to thousands of years following the K-Pg boundary (P0 Zone).

In Monmouth County, New Jersey, non-reworked ammonites were found in two successive 20 cm thick layers in the top of the Tinton Formation above an iridium enrichment that could represent the K-Pg boundary level, but discussion remains whether the iridium may have migrated downwards. In the lowest of the two beds, the Pinna Layer, the ammonite fauna is dominated by, but not uniquely composed of, heteromorphs; 4 species of scaphitid *Discoscaphites* and 2 species of baculitid *Eubaculites*. In the overlying Burrowed Unit, *Discoscaphites* and *Eubaculites* are the only ammonite genera recorded.

Because nearly all these possible survivors are heteromorph ammonites, and heteromorphs were frequently linked with ammonite extinction, a review on these occurrences was added as a chapter in a multiauthor review paper on the paleobiology of heteromorph ammonites, half a century after Jost Wiedmann's seminal paper in the same journal Biological Reviews (Hoffmann et al, 2021).

At current, the factors controlling this short-term survival are not well understood. Remarkably, all three areas related to the scaphitid-baculitid cluster and are relatively shallow water sites (estimated to be below <100m water depth).

3.4.4) Heteromorph ammonites and ammonite extinction

An important part of the late Cretaceous ammonite faunas is heteromorph ammonites. Of only 3 of the 33 terminal Maastrichtian ammonite sites, heteromorphs are unrecorded, and if the model of figures 4.2-4.5 is correct, heteromorphs would have probably present in all sites and their absence in the three sites is a matter of current collecting bias.

Heteromorph ammonites have been frequently linked to the extinction of the ammonoids, especially in older literature. Their 'aberrant' shell shapes, with aberrant meaning different but with a negative connotation, not in the least in French and German, were often related with degeneration, typolysis and phylogenetic extinction. The fact that heteromorphs were also abundant in many Cretaceous deposits, and even the most dominant faunal element in many late to latest Cretaceous ammonite faunas, sustained these hypotheses.

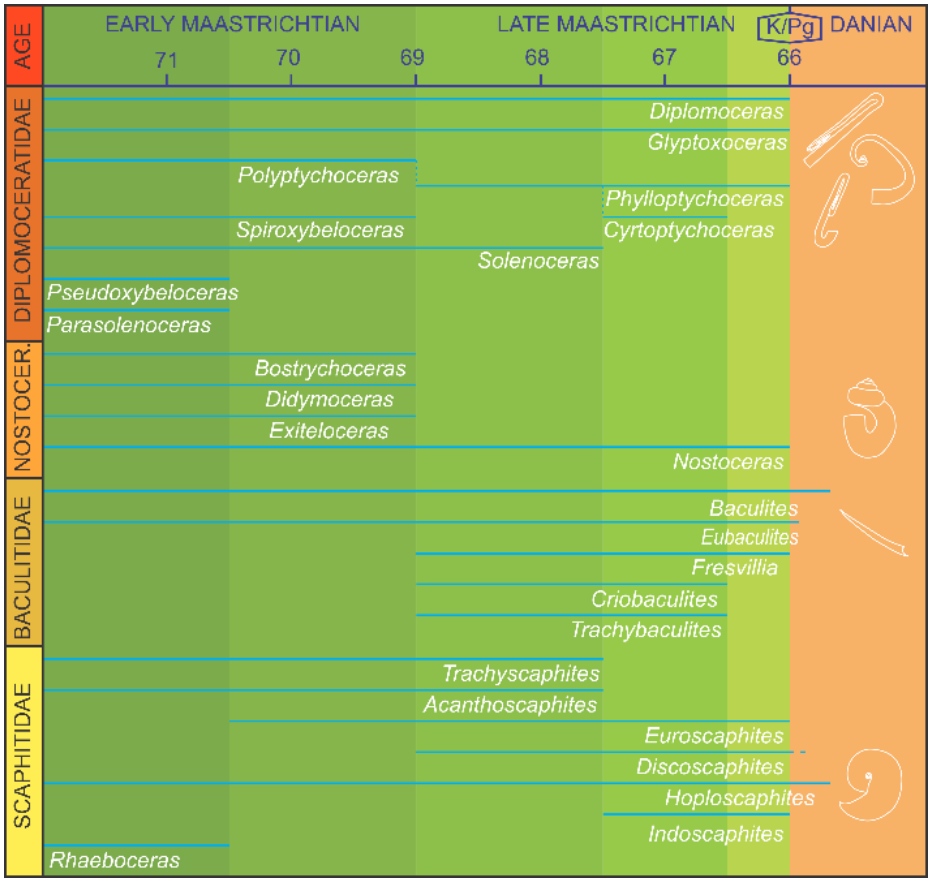

Figure 18. Range of heteromorph ammonite genera throughout the Maastrichtian and earliest Danian (taxonomy after Treatise, with the omission of *Jeletzkytes* and *Karlwaageites* and of the subgenus *Tovebirkelundites*. In absence of a fully integrated stratigraphic scheme for the subdivision and correlation of all basins, the division of the Maastrichtian into the five bins (early early, late early, early late, late late and last 0.5 myr) is arbitrarily. Phylogenetic relationships between the different scaphitid genera differ over different authors and were therefore not drawn. (From Hoffmann et al., 2021).

Of the 31 genera that are recorded from these 33 sites, 11 (nearly 1/3) are heteromorph. Our review (Hoffmann et al. 2021) also revealed that heteromorphs still evolved within the

Maastrichtian, the last stage of the Cretaceous; new genera developed within the Diplomoceratidae, Baculitidae and Scaphitidae (Fig. 4.7). The Nostoceratidae however reveal clear signs of demise, no new genera developed, and their entire late Maastrichtian record exists out of 2 very small *Nostoceras* sp. specimens from the Maastrichtian type are (The Netherlands, Belgium).

3.4.5) Nautilid turnover across the K-Pg boundary

The 'nautilid side of the K-Pg boundary crisis story' was never thoroughly investigated and remained one of the last unexplored issues of the K-Pg boundary biotic crisis. Very little is known about how nautilids responded to the environmental stresses prior to, at, and shortly after the Chicxulub impact. This is largely due to the lack of easy access to occurrence data (space and time) and the current state of their taxonomy, in particular at the species level, which is largely outdated.

In general, nautilid fossils are very rare in nearly all K-Pg boundary sections. For example, at the well-studied site of Kalaat Senan, Tunisia, only a single nautilid was found amongst 800 ammonoids in the topmost meters of the Maastrichtian. The same holds true for most of the ammonoid bearing K-Pg boundary sites. However, one notable exception exists. In Europe, a fairly large number of sites preserve abundant and relatively well-preserved nautilid fossils that have already been collected and await study in several natural history museums, universities, and research facilities across Europe.

Studying these collections revealed that next to more specimens, the European sections generally also have a high(er) number of co-occurring species, so that Europe may hold the key to further our understanding of the survival of the nautilids. More importantly, studying these collections allowed to bring together many data on the occurrences of nautilids in uppermost Cretaceous to lowermost Paleogene sediments, to resolve part of the outdated species level taxonomy, as well as to assemble a large dataset of shell parameters of the occurring species. And last but not least, it also allowed to identify a number of key sections in France, Belgium, The Netherlands, Denmark and Sweden. Here, nautiloid faunas from below and above the K-Pg boundary are quite different, providing strong evidence of a major response to the changing conditions. Apparently, nautilids did experience a major evolutionary turnover across the K-Pg boundary, including (local and regional) extinctions of important morphotypes, in addition to migratory and speciation events amongst the surviving lineages.

Pinpointing the exact timing of the different events characterizing this turnover is not easy and is for a large part hampered by the extreme rarity of nautilid fossils in the first one to two million years of the Paleogene, not only in Europe, but in all parts of the world. Extensive searchers were executed in the collections of e.g. NHM (London, 2015), NRM (Helsinki, 2016), MfN (Berlin, 2016), MNHN (Paris, 2018) (funded by Synthesys), AMNH (2018, Collection Study Grant), NHMM (Maastricht) and RBINS (Brussels), and delivered less than a handfull of incomplete specimens. Only by the mid-Danian, nautilids reappear in large(r) numbers and diversity can again be assessed. Without resolving the timing issues, correlating the observed changes in nautilid faunas with major disrupters of that time like the Chicxulub impact or Deccan flood basalt volcanism remains unclear.

At current, there are still some taxonomical problems remaining that hamper our work. These problems cannot be resolved by conventional methods, largely because too few shell parameters can be measured on the outer surface of these specimens, and for several globular shell shapes, correct measurements by caliper display a large margin of error. The most powerfull method to overcome this is to microCT scans a large number of specimens and advance from there. The microCT scanning is currently being executed within the scope of DiSSCo-Fed and the research will be continued within WP1 of the new project B2/191/P2/CT-CEPH that focusses on the Belgian fossil record of Nautilids based on microCT scanning of RBINS and RMCA specimens. Some early results were communicated at the 10th ISCPP in april 2018 in Fez, Morocco [Goolaerts, 2018] and at a lecture for broader audience in 2019. Other more extensive reports are in preparation.

3.4.6) Other molluscs: gastropods and bivalves

A quantitative analysis [Vellekoop et al. 2020] was performed on systematically sampled macrofossils of the topmost Maastrichtian and lowermost Danian beds at the Curfs quarry near Maastricht, each representing 'snapshots' of the latest Cretaceous and earliest Palaeogene marine ecosystems respectively of the type Maastrichtian area. In these beds, molluscs like gastropods and bivalves are diverse and abundant, next to common ammonites, and far less common nautiluses and belemnites. Regional ecosystem changes across the K-Pg boundary were concluded to be relatively minor, showing mostly a decline in suspension feeders, accompanied by an ecological shift to endobenthic molluscs. The earliest Paleocene gastropod assemblage retained many 'Maastrichtian' features and document a fauna that temporarily survived into the early Danian (Fig. 19). We concluded that the local setting, this is the shallow oligotrophic carbonate platform may have played a major role in the quick local recovery of the ecosystem, presumably especially inhabited by taxa that were already well adapted to low nutrient levels giving them a better resistance to starvation. As a result, we concluded that the local taxa were less affected by the short-lived detrimental conditions related to K-Pg boundary perturbations, such as darkness, cooling, starvation, and ocean acidification resulting in relatively high survival rates, enabling rapid recolonization and recovery of marine faunas in the Maastrichtian type area.

It is at present uncertain whether the same reasoning can be extrapolated to the freeswimming ammonites and nautiluses. For the ammonites, the fauna from just below and above the K-Pg boundary in the type Maastrichtian is also somewhat different in composition, in particular in the baculitids, but in general fairly similar, like the ratio scaphitids versus baculitids. Why then shortly after these ammonites dissapear completely is not yet understood. The same question holds for the gastropods, after the quick recovery of the ecosystem, a second and much major diversity change occurred somewhere between the earliest Danian and mid-Danian, and no fossils are known in the area in between these two levels.

3.4.7) Crustaceans across the K-Pg boundary

Interesting results came also from the study of a suite ciripede remains in the vicinity of the K-Pg boundary in Tunisia, a study that was executed in close collaboration with taxonomers of this group Andy Gale (Portsmouth, UK) and John Jagt (NHMM) [Gale et al, 2021]. We were able to describe an assemblage of large and robust pedunculate scalpellomorph cirripede barnacles from the Maastrichtian of Kalaat Senan, and document four taxa, three of which

are confined to the Kalaat Senan area and one which had been recorded only from the Maastrichtian of the Farafrah Oasis in the Western Desert of Egypt. One of these species is new to science, namely *Cretiscalpellum robaszynskii*, named after dr. Francis Robaszynski, Professor emeritus of the Universite de Mons (Belgium), eminent stratigrapher, micropalaeontologist and field geologist, for his tireless efforts in the study of the Cretaceous as a whole and the Tunisian Cretaceous in particular (Fig. 20). These new finds yield interesting clues to the evolution of the composition of North African cirripede assemblages during the early and late Maastrichtian, up close to the K-Pg boundary mass extinction. The fauna comprises remarkably large-sized and strongly armoured forms for the supposedly offshore open-marine palaeoenvironment of Kalaat Senan, a faunal character that seems to have developed after the Campanian and disappeared by the Danian. The presence of *Pachyscalpellum*, a genus that was previously restricted to Australasia, indicates faunal connections with the eastern Tethys. Their documented first arrival coincides roughly with the first documented occurrence of the North American scaphitid ammonite genus *Discoscaphites*.

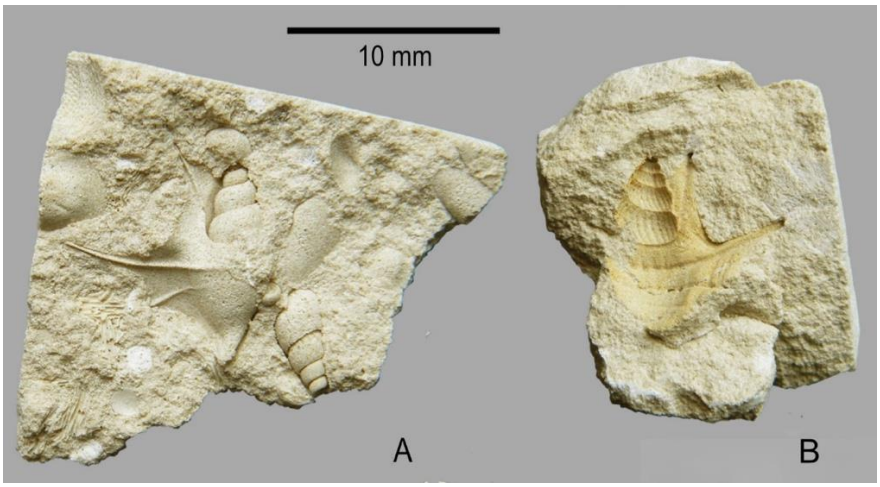

Figure 19. While the aporrhaid gastropod *Aporrhais limburgensis* is the dominant gastropod in the assemblage of the uppermost Maastrichtian unit IVf6 (A), it also occurs albeit much rarer in the lowermost Paleocene unit IVf7 (B) where it is mostly replaced by *Arrhoges* (*Latiala*) *pelecyphora* (after Vellekoop et al., 2000, modified).

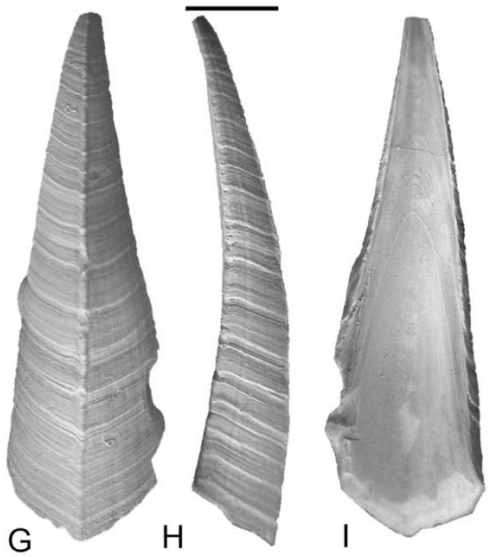

Figure 20. The holotype (carina plate) of the newly described cirripede species *Cretiscalpellum robaszynskii* Gale Jagt and Goolaerts 2021 from the late Maastrichtian of Tunisia. Scale bar equals 5 mm. [from Gale et al., 2021]

Fifth objective: the effect of impact and volcanism on the evolution of planets, mantle and atmosphere – *WORK PACKAGE 5* –

Chicxulub is the only large terrestrial crater with a perfectly preserved peak-ring and therefore a unique source of information to understand the formation process of this feature, also observed on extraterrestrial craters (e.g. Schrödinger, Moon). Based on the data recovered during our 2016 core description, Morgan et al. (2016) showed that the shocked granites (> 10 GPa) display a low density, high porosity and contain numerous dikes, cataclastic shear, shear-zones and brittle deformation. These evidence of brittle and viscous deformations attest of acoustic fluidization process during the upward transport of the deep-rooted granite (± 10 km, Riller et al. 2018) and explain the measured low P-wave velocities (Christeson et al. 2018). These observations are fully compatible with a peak-ring formation according to the "dynamic collapse" theory predicted by numerical modeling, rather than the field based "nested-melt cavity" model proposed for large crater formation. The impact trajectory (angle and direction) is reconstructed based on the information extract from IODP-ICDP core and asymmetries in the subsurface structure of the Chicxulub crater (Collins et al. 2020). Comparison of 3D numerical simulations of Chicxulub-scale impacts with geophysical observations suggests that the Chicxulub crater formed by a steeply-inclined (45–60° to horizontal) impact from the northeast. A steeply inclined impact produces a nearly symmetric distribution of ejected rock and releases more climate-changing gases per impactor mass than either a very shallow or near-vertical impact, which is compatible with the observation (Claeys et al. 2002)

Large impact events excavate mid- to lower-crustal rocks, offering a unique perspective on the interior composition and tectonic history (if any) of planetary bodies. On the Yucatán Peninsula, México, the surface geology mainly consists of sedimentary rocks, with a lack of exposure of crystalline basement in many areas. Consequently, current understanding of the Yucatán subsurface is largely based on impact ejecta and drill cores recovered from the ~200-km-diameter Chicxulub impact structure. In this project we obtained together with colleagues at University of Texas, Austin, the first apatite and titanite U-Pb ages for pre-impact dacitic, doleritic, and felsitic magmatic dikes preserved in Chicxulub's peak ring sampled during the 2016 IODP-ICDP Expedition 364 (De Graaff et al. submitted). Dating yielded two age groups, with Carboniferous aged dacites (326–317 Ma) and a felsite (342.5 ± 4.3 Ma) overlapping in age with most of the granitoid basement, as well as Jurassic dolerites (168–158 Ma) and a felsite (152.2 ± 11.4 Ma) that represent the first in-situ sampling of Jurassic-aged crystalline basement for the Yucatán Peninsula. The Nd, Sr, and Hf isotopic compositions of the pre-impact lithologies and impact melt rocks indicate that dolerites potentially contributed to up to ~40 vol% of the Chicxulub impact melt. This percentage implies that the dolerites comprised a large part of the Yucatán subsurface by volume, representing a hitherto unsampled pervasive Jurassic magmatic phase. We interpret this magmatic phase to be related to the opening of the Gulf of Mexico, likely constraining its onset to the Late Middle Jurassic (de Graaff et al. submitted).

Impact cratering forms the most common geological process in the Solar System. As a well-preserved terrestrial ground truth, Chicxulub provides an accessible site to test in the field, remote-sensing observations made on other planetary bodies. Its study improves our understanding of crater formation on solid planetary surfaces, by favoring the dynamic

collapse model; it documents crater impactite and ejecta relationships facilitating landing site location; also the connection between crater morphology and impactites may help select optimal sampling location on Mars or other planets. Hydrocode modeling and derived atmospheric perturbation scenarios tested at Chicxulub are applicable to other planets. Indeed, some of the lessons learned from Chicxulub are currently being applied to learn about the cratering process, and its consequences on early evolution of Mars and ROB scientists use it to constrain data obtain from the DART mission, and (in the future) Hera missions, which are part of the ESA – NASA planetary defense program.

BIBLIOGRAPHY:

Alvarez, et al., *Science* 208, no. 4448, 1095-1108, 1980.
Alvarez, et al., *Geology*, v. 20, p. 697-700, 1992.
Alvarez et al., Science, 269, 930-935, 1995.
Artemieva et al. *Geophysical Research Letters*, 44, 70, 10180-10188, 2017
Belcher, et al. *Proceedings of the National Academy of Sciences, USA,* 106, 4112-4117, 2009.
Bohor, et al., *Science* 224, no. 4651, 1984.
Binkowski, and Shanker, *Journal of Geophysical Research: Atmospheres* 100, 26191-26209,1995.
Brugger et al., *Geophysical Research Letters*, 44, 1, 419-427, 2017
Chou, and Suarez, *A solar radiation parameterization for atmospheric studies, NASA, 1999.*
Chou, et al. *A thermal infrared radiation parameterization for atmospheric studies, NASA, 2001.*
Claeys et al. *Geological Society of America, SP* 356, 55-68, 2002
Claeys, Ph., et al., *Meteorit. & Planet. Sci*. 38, 1299-1317, 2003
Collins et al. *Nature communications* 11, 1-10, 2020.
Christeson et al. *Earth and Planetary Science Letters*, 495, 1-11, 2018
Davis et al. Montly Weather Review, 136, 6, 1990-2005, 2008
De Graaff et al. *Geological Society of America Bulletin*, 134 (1-2): 293–3152022
DePalma et al. *Proceedings of the National Academy of Sciences, USA,* 116, 17, 8190-8199, 2019
Donovan, et al. *Nature Ecology & Evolution 1, 1-5, 2016.*
Dufresne et al. *Journal of the Atmospheric Sciences* 59, 1959-1966, 2002.
During et al. *Nature*, *603, 91-94, 2022.*
Emerson et al. *Proceedings of the National Academy of Sciences 117,* 26076-26082, 2020.
Feignon et al. *Meteoritics & Planetary Science*, 1-31, 2021
Feichter et al. *Bulletin of the American meteorological society* 79, 831-844, 1998.
Gale et al. *Cretaceous Research*, 118, 104650, 2021
Goderis et al. *Science Advances*, 7, 9, eabe3647, 2021
Goolaerts, Geological Society of America Abstracts with Program vol. 50 (6) 2018.
Gulick et al. *Proceedings National Academic of Science* USA, (39) 19342-19351, 2019
Hildebrand, et al., *Geology*, 19, 867-871, 1990.
Jimenez et al. Monthly Weather Review, 140, 3, 898-918, 2012
Kaiho, et al. *Scientific reports* 6, 1-13, 2016.
Kaskes, *Geological Society of America Bulletin*, 134, (3-4) 895-927, 2022
Kring and Durda, Journal of Geophysical Research: Planets, 107, E85062, 2002
Liu, et al. *Geoscientific Model Development 5, 709-739, 2012.*
Markwick,and Valdes, *Palaeogeography, Palaeoclimatology,Palaeoecology 213, 37-63, 2004.*
Morgan and Warner, *Geology*, 27, 407
Morgan, et al., *Nature*, 390, 472-476, 1997-410 1999.
Morgan et al. *Nature Reviews Earth&Environment*, 3, 338-354, 2022
Niezgodzki et al. Paleoceanography and Paleoclimatology, 32, 9, 980-998, 2017
Pierazzo, et al., *Journal Geophysical Research,* 103, no. E12 28607-2862, 1998.

Pierazzo, and Artemieva, *Elements* 8, no. 1, 55-60, 2012.
Pierrehumbert, and Gaidos, *The Astrophysical Journal Letters* 734, L13, 2011.
Pope, K. O, et al., *Earth Planetary Science Letters,* 170, 351-364, 1999.
Renne, et al., *Science*, 6256, 350, 76-78, 2015
Richards et al., *Geological Society of America Bulletin*. 127, 1507, 2015.
Richardson et al. *Geophysical Research Letters,* 112, E09001, 2007
Riller, et al., *Nature*, 562, 511-518, 2018
Ross et al. *Geological Society of America Bulletin,* 134 (1-2), 241-260, 2022
Schulte, et al., *Science*, 327, 1214-1218, 2010.
Senel, et al., *Journal of Geophysical Research: Planets*, *126*(10), e2021JE006965, 2021
Senel, et al. *Journal of Advances in Modeling Earth Systems* 11, 2655-2679, 2019
Senel et al. submitted to Nature Geosciences,
Smit, and Hertogen, *Nature* 285, no. 5762, 198-200, 1980.
Smit, and Kyte, *Nature* 310, 403-405, 1984.
Smit, et al., *Geology,* 20, 99-103, 1992.
Swisher, et al., *Science* 257, 954-958, 1992.
Tabor et al. *Geophysical Research Letters*, 47, 3, e601021, 2020
Temel et al. *Journal of Geophysical Research: Planets,* 126, 10, e2021JE006867
Tiedtke, et al. *Monthly weather review* 117, 1779-1800, 1989.
Toon et al., *Atmos. Chem. Phys. Discuss.*, 2016.
Tsarpalis, et al. *Remote Sensing* 10, 1595, 2018.
Urrutia-Fucugauchi, et al., *Meteorit. & Planet. Sci.* 39, 787-790, 2004
Vellekoop et al. Palaeontology 63(2), 349-367, 2020
Xu, and Carmichael, *Journal of Applied Meteorology and Climatology* 37, 1084-1099
Zhang, and Shao, *Atmospheric Chemistry and Physics,* 14, 12429-12440, 2014.
Zhao et al. *Gondwana Research*, 82, 128-150, 2020
Zhao et al. *Geology*, 49, 1-4, 2021

4. RECOMMENDATIONS

Take home message 1: The two identified melt-rock units record different episodes of crater formation, excavation, and modification stages, respectively. Importantly, the granites sampled in Hole M0077A are dissimilar in composition when compared to granite or gneiss clasts from other drill cores recovered from the Chicxulub impact structure. Marking them as valuable lithologies that provide new insight into the Yucatan basement (see below). The complex suevite depositonal sequence involves marine processes that affected this material as ocean rushed in the open cavity at the end of the modification stages, most likely. The presence of the elevated Ir anomaly within the very top of the sequence deposited on top of the peak-ring timely connects the formation of Chicxulub with the K-Pg boundary worldwide and demonstrates once for all the coincidence of the two events.

Take home message 2: Acoustic fluidization process drives the formation of large craters with pronounced topographic rings as illustrated by the dynamic collapse model (Morgan et al. 2016; Christeson et al. 2018). Over less than 10 minutes, the collision energy induces rapid and intense weakening of the target mid-crustal lithologies, followed by their significant upward flow to a level higher (km) than the initial surface (Riller et al. 2018), final collapse and rapid (re)consolidation of the rocks to sustain the newly formed rings.

Take home message 3: The deep-crustal lithologies brought up within the peak-ring sequence uplift provide a new view on the pre-impact tectonics of the Gulf of Mexico: A continental Carboniferous volcanic arc existed along the northern margin of the Maya block, before NW Gondwana collided with Laurentia, attesting of southward-directed subduction of Rheic oceanic crust beneath the Maya block. A detailed succession of the various magmatic/metamorphic and tectonic events and their timing from Precambrian to Jurassic is given in de Graaff et al. (Submitted to Lithos June 2022).

Take home message 4: our simulations show that the release of a massive plume of silicate dust with grain-sizes between ~1-10 µm was a key factor driving the K-Pg impact winter due to a long atmospheric lifetime for the dust of at least 20 years. The dust-induced photosynthetic shut-down, together with additional effects of soot and sulfur, led to the catastrophic collapse of primary productivity on land and in the ocean, steering the mass extinction in the direct aftermath of the Chicxulub impact.

Take home message 5: The work carried out shows that the response of different ecosystems to the impact generated perturbation can vary significantly. Different organisms react different to the cooling, dust, acid rain etc. The response of the biosphere is clearly not homogeneous and most likely varied very much based on ecosystem, organisms, local environment, and climate.

5. DISSEMINATION AND VALORISATION

The BELSPO Chicxulub project closed with a Public Outreach Event: June 23, 2022, at Museum of Natural Sciences, Brussels, titled: **From Asteroid Impact to Planetary Defense**
Registration Join our in-person public outreach event at the Royal Belgian Institute of Natural Sciences (RBINS) in Brussels on June 23, 2022, from 16:30 onwards, to gain exclusive insights from topical leaders in science and technology related to asteroid impacts and planetary defence!

Sponsored by ESA, ROB, RBINS, VUB-AMGC

https://www.facebook.com/ORBKSB/posts/5469580529752620

Invited lectures at scientific organizations:

- GEOTOP McGill University, Speaker Seminar, Montréal, Canada, October 25, 2022 (Ph. Claeys)
- Université du Québec à Montréal, Département Sciences de la terre et de l'atmosphère, Lecture, October 20, 2022 (Ph. Claeys)
- Physical Research Laboratory, Ahmedabad, India, Online Lecture, August 04, 2022 (Ph. Claeys)
- University of Brazilia, Institute of Geosciences, Online Lecture, September 29, 2021 (Ph Claeys)
- Koninklijke Nederlandse Akademie van de Wetenschappen (KNAW, Dutch Academy of Sciences), Lecture, Amsterdam, November 14, 2019 (Ph. Claeys)
- Belgian Association for Palaeontology, Lecture, Brussels, October 23, 2019 (Ph. Claeys)
- Ghent University, Dept. of Geology, Public lecture, Ghent, April 5, 2019 (Ph. Claeys)
- Collège Belgique, Académie Royale de Belgique, Namur, Lecture April 3, 2019 (Ph. Claeys)
- Northwest University, Dept. of Chemistry, Xi'An, China, Seminar March 29, 2019 (Ph. Claeys)
- Northwest University, Dept. of Geology, Xi'An, China, Lecture March 28, 2019 (Ph. Claeys)

- Université du Québec à Montréal, Département Sciences de la terre et de l'atmosphère, Lecture, November 8, 2018 (Ph. Claeys)
- Trinity College, Dublin, John Joly Memorial Lecture 2018, February 8, 2018 (Ph. Claeys)
- GeoTop McGill University, Speaker Seminar, Montréal, October 19, 2017 (Ph. Claeys)

Public lectures:

- March 10, 2018: Waarom nautilussen het overleefden ammonieten niet? PaleoTime-Nl te Ede, Nederland, public lecture: 60 people (Stijn Goolaerts)
- November 24, 2018: Wanneer Krijt geen krijt is. Themadag Krijt van de Nederlandse, Geologische Vereniging, te Utrecht, Nederland, public lecture 150 people (Stijn Goolaerts)

Press and media:

- 24.12.2021. Interview RTL TVI 19:00 news with O. Karatekin. https://www.rtl.be/info/video/797235.aspx
- 24.12.2021 TV Interview RTBF 19:30 evening news with O. Karatekin, https://www.rtbf.be/auvio/detail_nasa-mission-lancee-pour-devier-la-trajectoire-d-un-asteroide?id=2835492
- 24.12.2021, Radio interview with O. Karatekin https://louizradio.be, 24/122/2021.
- 23.12.2021 Written Press on nrc : https://www.nrc.nl/nieuws/2021/12/23/biljarten-met-66-kilometer-per-seconde-om-ooit-een-botsing-te-voorkomen-a4066503
- 29.12.2021 TV Interview with BX1 with O. Karatekin. https://bx1.be/categories/news/lobservatoire-royal-de-belgique-participe-a-une-mission-de-defense-planetaire-avec-la-nasa/
- 15.06.2021, EOS article about the new ages presented on the Chicxulub granite (published in Ross et al., 2021). https://eos.org/articles/vestiges-of-a-volcanic-arc-hidden-within-chicxulub-crater
- 26.02.2021, Global news coverage of our Science Advances paper "Globally distributed iridium layer preserved within the Chicxulub impact structure" on the settling of iridium within the Chicxulub impact structure: vrt.be, RTBF, De Standaard, HLN, Forbes, Physics World, Science & Avenir, Yahoo News, Süddeutsche Zeitung, Sky TG24 etc.
- 06.01.2021 : Newpsaper article : La Libre Belgique : La vraie mission "Armageddon": Comment l'Esa et la Nasa veulent protéger la Terre contre les astéroïdes 6/01/2021, https://www.lalibre.be/planete/sciences-espace/2021/01/06/la-vraie-mission-armageddon-comment-les-etats-unis-et-leurope-veulent-proteger-la-terre-contre-les-asteroides-MQE3AM26LVFBDGEZTGT6IFZMCA/
- 01.01.2020, Science list our research on the Chicxulub crater and dinosaur mass extinction as among the top runners up for Science Breakthrough of the year 2019, http://science.sciencemag.org/content/366/6472/1436
- 01.11.2019 knack opinie: Dinosauriërs waren de bekendste slachtoffers van de meest recente massaextinctie', 2 pages article in Knack, Flemish news magazine covering release of video: by "Universiteit van Vlaanderen": Hoe zijn de dinosaurussen nu echt uitgestorven (how did dino's really died).
- 09.09.2019 Worldwide Press, coverage of our article in PNAS, The first day of the Cenozoic, on the mechanisms that led to the demise of the dinosaurs after the Chicxulub impact published in RTBF news, National Geographic, The Smithsonian, Wall Street Journal, El Païs, Il Post, New York Times etc.

- 31.05.2018, News cover of our Nature paper, Rapid recovery of life at ground zero of the end Cretaceous mass extinction, showing how quickly life return into the Chicxulub crater in Yucatán, 7Sur7.be, VRT News, Het Laatste Nieuws, La Dernière Heure, RTL Info, Science & Avenir, Science News, Discovery Magazine, etc.
- 02.06.2017, Peter Wall In for Advanced Studies Newsletter, Article "The impact of impacts", by David Morrison on ongoing research based on recent drilling of the Chicxulub crater in Yucatan (http://www.pwias.ubc.ca/wall-papers/the-impact-impacts)
- 23.05.2017, May edition of EOS Wetenschap (Dutch/Flemish popular science magazine), article "In een uur was de wereld compleet veranderd" based interview related to research on the Cretaceous-Paleogene mass extinction
- 15.05.2017, BBC news article "Dinosaur asteroid hit 'worst possible place" promotion of BBC documentary "the day the dinosaurs died", http://www.bbc.com/news/science-environment-39922998

Video and documentaries:

- Universiteit van Vlaanderen, educational video presentation titled : *Hoe zijn de dinosaurussen nu echt uitgestorven* (how did dino's really died), https://www.universiteitvanvlaanderen.be/college/hoe-zijn-dinosaurussen-nu-echt-uitgestorven/
- Participation to BBC Documentary "*The day the dinosaurs died*" aired first on 16.05.2017, see https://vimeo.com/218496418 or https://www.pbs.org/video/day-dinosaurs-died-sytqgj/ https://www.youtube.com/watch?v=Id-M1lerGDQ (shown on PBS in USA, etc.)
- Participation to documentary "Science Grand Format" France 5, Le jour où les dinosaures ont disparu", https://www.france.tv/documentaires/science-sante/311357-le-jour-ou-les-dinosaures-ont-disparu.html

Presentation/poster at Scientific Conferences (project members in bold):

European Geosciences Union General Assembly 2022, Vienna

- **Senel, C. B., Temel, O., & Karatekin, O.** (2022). Probing Martian turbulence kinetic energy and dissipation rate during major dust storms. Vienna, Austria, 23-27 May.

Europlanet Science Congress 2022, Granada

- Senel**, C. B., & Karatekin, O.** (2022). Hypervelocity impact simulations of DART on asteroid Dimorphos: Impact-generated porosity and gravity anomalies. Session: Latest Science Results in Planetary Defence, Granada, Spain, 18-23 September.

Lunar and Planetary Science Conference, Houston TX, 2022

- **Kaskes, P., Stennik, M., Goderis, S., Tagle, R.,** Smit, J. **& Claeys, P.,** High-Resolution Chemostratigraphy of the Cretaceous-Paleogene (K-Pg) Boundary Interval in the US Western Interior: Implications for Chicxulub Impact Ejecta Dynamics, High-Resolution Chemostratigraphy of the Cretaceous-Paleogene (K-Pg) Boundary Interval in the US Western Interior: Implications for Chicxulub Impact Ejecta Dynamics. Houston: Lunar and Planetary Institute, Vol. 2022. p. 1-2.
- **Kaskes, P., De Graaff, S. J.**, Feignon, J-G., **Dehais, T., Goderis, S.**, Ferrière, L., Koeberl, C., Smit, J., Wittmann, A., Gulick, S. P., Debaille, V., Mattielli, N. & **Claeys, P.**, The Drill Core Diary: Unravelling the Rapid Emplacement of Suevite and Impact Melt Phases Within the Chicxulub Impact Structure. Lunar and Planetary Institute, p. 1-2 2 p.

Meteoritical Society meeting, Glasgow, 2022

- Feignon, J-G, Schultz, T., Ferriere, L., **Goderis, S., De Graaff, S.J., Kaskes, P., T. Déhais, Claeys, Ph**., Koeberl, C., Lack of ubiquitous impactor component in the Chicxulub peak-ring impact melt rock: Implications for the fate of the projectile, 85th Annual Meeting of the Meteoritical Society 2022 LPI Contribution 2695.

Geological Society of America 2021

- **Claeys, P., , De Graaff, S. J., Dehais, T., Sinnesael, M. & De Winter, N.,** 12 Aug 2021, From Gubbio to Chicxulub: k-pg iridium anomaly comes full circle. Geological Society of America, p. 1-1 1 p.
- **De Graaff, S. J., Kaskes, P., Dehais, T., Goderis, S.**, Debaille, V., Ross, C., Gulick, S. P., Feignon, J-G., Ferrière, L., Koeberl, C., Smit, J., Mattielli, N. & **Claeys, P**., 12 Aug 2021, new insights into the formation and emplacement of impact melt rocks within the chicxulub impact structure, following the 2016 iodp-icdp expedition 364. Geological Society of America, p. 1-1 1 p.
- Faucher, J., **Dehais, T., Kaskes, P., De Graaff, S. J.**, Lambert, P., Luais, B. & **Goderis, S.**, 12 Aug 2021, First petrographic and geochemical characterization of impact melt-rich lithologies and target rocks within the rochechouart impact structure (france), recovered by the 2017 drilling campaign. Geological Society of America, p. 1-1 1 p.
- Feignon, J-G., Schulz, T., Ferrière, L**, De Graaff, S. J., Kaskes, P., Dehais, T., Claeys, P.** & Koeberl, C., 12 Aug 2021, Do the impact melt rocks within the chicxulub impact structure peak ring (Yucatan peninsula, Mexico) preserved an impactor signature?. Geological Society of America, p. 1-1 1 p.
- **Kaskes, P., De Graaff, S. J.**, Feignon, J-G**., Dehais, T., Goderis, S.**, Ferrière, L., Koeberl, C., Smit, J., Wittmann, A., Gulick, S. P., Debaille, V. & Mattielli, N., **Claeys, Ph**. Suevite emplacement within the Chicxulub impact structure: new insights from the 2016 iodp-icdp expedition 364 drilling. Geological Society of America, p. 1-1 1 p.
- Ross, C., Stockli, D. F., Gulick, S. P., **Kaskes, P**., Smit, J. & Artemieva, N., 12 Aug 2021, Finding a specific needle in a haystack: tracing ejected zircon from the Chicxulub impact in k-pg boundary sections. Geological Society of America, p. 1-1 1 p.
- Senel, C. B., Temel, O., **Kaskes, P., Vellekoop, J., Goderis, S.**, Van Hove, B. & Karatekin, O., 12 Aug 2021, Relative roles of impact-generated aerosols on photosynthetic activity following the Chicxulub asteroid impact. Geological Society of America, p. 1-1 1 p.
- **Vellekoop, J., Kaskes, P.**, Smit, J., Speijer, R. & **Claeys, P.,** 12 Aug 2021, Rapid biological recovery following the cretaceous-paleogene boundary catastrophe in the Maastrichtian type area. Geological Society of America, p. 1-1 1 p.

Meteoritical Society Meeting, Tucson, Arizona 2021

- Feignon, J-G., Schulz, T., **Goderis, S., De Graaff, S. J., Kaskes, P., Dehais, T., Claeys, P.** & Koeberl, C., 2 Jul 2021, EXAMINING THE (POTENTIAL) PRESENCE OF A PRESERVED Impactor signature in the impact melt rocks of the Chicxulub structure peak-ring. Meteoritical Society, Tucson, Arizona, USA, p. 1-1 1 p.

European Geosciences Union General Assembly 2021, Vienna

- **Huygh, J. J., Vellekoop, J., Sinnesael, M., Kaskes, P.**, Jagt, J. W. M. & **Claeys, P**., Cyclostratigraphy of a type-Maastrichtian chalk record, based on high-resolution geochemical analysis of the Gulpen Formation, NE Belgium EGU General Assembly 2021 Conference Abstracts. EGU General Assembly Conference Abstracts, p. 4806-4806 1 p.

- Van Dijk, J., Sepúlveda, J., Alegret, L., Birch, H., Bralower, T., Jones, H., Henehan, M., Hull, P., Negra, M. H., Ridgwell, A., Röhl, U., **Vellekoop, J**., Westerhold, T., Whiteside, J. & Zeebe, R., The recovery of the biological pump across the K-Pg boundary in the GSSP of El Kef, Tunisia, EGU General Assembly 2021 Conference Abstracts. EGU General Assembly Conference Abstracts, p. 8200-8200 1 p.
- Vancoppenolle, I., **Vellekoop, J.,** Doubrawa, M., **Kaskes, P., Sinnesael, M.**, Jagt, J. W. M., **Claeys, P.** & Speijer, R., 3 Feb 2021, EGU General Assembly 2021 Conference Abstracts. EGU General Assembly Conference Abstracts, p. 2182-2182 1 p.

Geological Belgica 2021 AfricaMuseum Tervuren

- **Dehais, T., De Graaff, S. J., Goderis, S. & Claeys, P.**, 26 Aug 2021, Latest developments in micro-X-ray fluorescence (µXRF) analysis in geosciences: high-resolution element mapping, digital image analysis, and quantifications. Geologica Belgica: 7th INTERNATIONAL GEOLOGICA BELGICA MEETING 2021. Tervuren, Belgium: Royal Museum for Central Africa, p. 246-247 2 p.
- Vancoppenolle, I., **Vellekoop, J.,** Doubrawa, M., **Kaskes, P., Sinnesael, M.**, Jagt, J. W. M., **Claeys, P.** & Speijer, R. P., Sep 2021, Geologica Belgica: 7th INTERNATIONAL GEOLOGICA BELGICA MEETING 2021. Tervuren, Belgium: Royal Museum for Central Africa, p. 212-213 2 p.
- **Vellekoop, J.,** Rapid biological recovery following the Cretaceous-Paleogene boundary catastrophe in the Maastrichtian type area, Geologica Belgica: 7th INTERNATIONAL GEOLOGICA BELGICA MEETING 2021. Tervuren, Belgium: Royal Museum for Central Africa, p. 214-215 2 p.

Lunar and Planetary Science Conference, Houston TX, 2021

- Feignon, J-G**., De Graaff, S. J.**, Ferrière, L., **Kaskes, P., Dehais, T., Goderis, S., Claeys, P.** & Koeberl, C., 29 Jan 2021, 52nd Lunar and Planetary Science Conference 2021: LPI Contrib. No. 2548. Lunar and Planetary Institute, p. 1557-1557 2 p.

European Geosciences Union General Assembly 2021, Vienna

- **Vellekoop, J., Kaskes, P., Sinnesael, M.**, Jagt, J. W. M., Speijer, R. & **Claeys, P**., A chemostratigraphic framework for the type-Maastrichtian, EGU General Assembly Conference Abstracts 2020: EGU2020-13863. p. 13863-13863 1 p.

Large Meteorite Impacts VI meeting, 2019, Brasilia (4 oral communications), Lunar and Planetary Institute Contribution 2136, (https://www.hou.usra.edu/meetings/lmi2019/)

- **Déhais, T., Kaskes, P., de Graaff, S.J.**, Chernonozhkin S.M., Debaille, V., Vanhaecke F., **Claeys, Ph. Goderis,** S. Disantangling cratering processes using non-traditional isotopes on core M0077A of the IODP-ICDP Exp. 364 in the Chicxulub structure #5106
- **De Graaff, S. J., Kaskes, P., Déhais, T., Goderis, S**., Debaille, V., Feignon, J-G., Ferrière, L., Koeberl, C., Ross, C., **Claeys, Ph**. Making (more) sense of destruction – a comprehensive geochemical investigation of Chicxulub impactites recovered during IODP_ICDP expedition 364, #5079
- **Goderis, S.** Sato, H., Ferrière, L., Schmitz, B., Burney, D., Bralower, T. J., **De Graaff, S. J., Déhais, T., De Winter, N.**, Elfman, M., Feignon, J-G., Gulick, S. P. S., Ishikawa, A., **Kaskes, P.**, Koeberl, C., Kristiansson, P., Lowery, C. M., Morgan, J., Neal, C. R., Owens, J. D. & 9 others, The final settling of meteoritic matter on the peak-ring of the chicxulub impact structure at site m0077a of iodp-icdp expedition 364. Large Meteorite Impacts VI 2019

(LPI Contrib No. 2136): Abstract 5068. Houston, TX: Lunar and Planetary Institute, Vol. 6. p. 1-2 2 p. 5068

- **Kaskes, P., De Graaff, S.J., Déhais, T., Goderis**, S. Feignon, J-G, Ferriere, L., Koeberl, C., Smit, J., **Claeys, Ph**., Geochemical and petrographic characterization of the suevite sequence within the IODP-ICDP exp. 364 core of the Chicxulub peak ring, #5085
- **Kaskes, P., Goderis, S., Belza, J.,** Tack, P., DePalma, R. A., Smit, J., Vincze, L., Vanhaecke, F. & **Claeys, P.,** Caught in amber: geochemistry and petrography of uniquely preserved Chicxulub microtektites from the Tanis K-Pg site from North-Dakota (USA), #5090

7th International Academy of Astronautics (IAA) Planetary Defense Conference, 2021

- **Senel C.B., Temel O., & Karatekin O.** (2021). Environmental consequences of asteroid impacts by GCM simulations. *Virtual meeting,* 26-30 April.

European Geosciences Union General Assembly 2020, Vienna

- Sert, H., **Temel, O., Berk Senel, C., & Karatekin, O.** (2020). A global circulation model for the asteroid impact simulations. In European Geoscience Union (EGU) General Assembly, virtual, 4-8 May**.**

European Geosciences Union General Assembly 2019, Vienna

- Feignon, J-G., Ferriere, L., Koeberl, C., **De Graaff, S. J., Kaskes, P., Goderis, S., Déhais, T. & Claeys,** P., Geochemistry and petrography of granitoid basement from the Chicxulub peak-ring, p.10791
- **Ozgür Karatekin, Orkun Temel**, Idealized Simulation of Ocean Acidification after the Cretaceous–Paleogene extinction event p. 16854

Lunar and Planetary Science Conference, Houston TX, 2019

- **De Graaff, S. J., Kaskes, P., Déhais, T., Goderis, S.**, Debaille, V., Feignon, J-G., Ferrière, L., Koeberl, C., Ross, C. & **Claeys, P**., MAKING (MORE) SENSE OF DESTRUCTION – A COMPREHENSIVE GEOCHEMICAL INVESTIGATION OF CHICXULUB IMPACTITES RECOVERED DURING IODP-ICDP EXPEDITION 364. Large Meteorite Impacts VI 2019. Houston, TX: Lunar and Planetary Institute, Vol. 6. p. 1-2 2 p. 5079
- Déhais, T., Kaskes, P., De Graaff, S. J., Chernonozhkin, S., Debaille, V., Vanhaecke, F., **Claeys, P. & Goderis, S.**, DISENTANGLING CRATERING PROCESSES USING NON-TRADITIONAL ISOTOPE RATIOS ON CORE M0077A OF THE IODP-ICDP EXPEDITION 364 IN THE CHICXULUB IMPACT STRUCTURE, Large Meteorite Impacts VI 2019 (LPI Contrib No. 2136): Abstract 5106. Houston, TX: Lunar and Planetary Institute, Vol. 6. p. 1-2 2 p. 5106
- **Kaskes, P., de Graaff, S., Déhais, T., Goderis, S.**, Feignon, J-G., Ferrière, L., Koeberl, C., Smit, J. & **Claeys, P.**, GEOCHEMICAL AND PETROGRAPHIC CHARACTERIZATION OF THE SUEVITE SEQUENCE WITHIN THE IODP-ICDP EXP. 364 CORE OF THE CHICXULUB PEAK RING, Large Meteorite Impacts VI 2019 (LPI Contrib. No. 2136): Abstract 5085. Houston, TX: Lunar and Planetary Institute, Vol. 6. p. 1-2 2 p. 5085
- **Kaskes, P., Goderis, S., Belza, J.,** Tack, P., DePalma, R. A., Smit, J., Vincze, L., Vanhaecke, F. & Claeys, P., CAUGHT IN AMBER: GEOCHEMISTRY AND PETROGRAPHY OF UNIQUELY PRESERVED CHICXULUB MICROTEKTITES FROM THE TANIS K-PG SITE FROM NORTH-DAKOTA (USA) Large Meteorite Impacts VI 2019 (LPI Contrib. No. 2136): Abstract 5085. Houston, TX: Lunar and Planetary Institute, Vol. 6. p. 1-2 2 p. 5090

Geological Society of America Annual Meeting 2018, Indianapolis, USA

- **Goolaerts, S.**, 2018. Towards a paleoecological and paleogeographical model for ammonoids during Deccan volcanism. Geological Society of America Abstracts with Program vol. 50 (6). doi: 10.1130/abs/2018AM-321991. [Talk presented at 11.30 on Nov 6 2018 at GSA annual meeting in Indianapolis in Session T123. Cephalopods through time]

American Geophysical Union Meeting 2018, Washington DC

- **De Graaff, S. J., Kaskes, P., Déhais, T., Goderis, S. & Claeys, P.,** Making sense of destruction Geochemistry of the Chicxulub impact melt rocks and granitoid target, recovered during IODP-ICDP Expedition 364 Abstract 368103
- **Kaskes, P., De Graaff, S. J., De Winter, N., Déhais, T**., Smit, J., Goderis, S. & Claeys, P., Geochemical fingerprinting of target lithologies within the Chicxulub impact breccia, Abstract 453195

EGU 5th Galileo Mass-Extinctions, Recovery & Resilience August 2019, Utrecht

- **Goolaerts, S.** Ammonite death and nautilus survival at the Chicxulub massacre: here's what we know so far. Abstract book GC5-Mass-53.
- **Vellekoop, J**., Van Tilborgh K.H., Van Knippenberg, P, Jagt, J.W.M., Stassen, P., **Goolaerts S**., Speijer, R. P., 2019. Rapid biological recovery following the Cretaceous-Paleogene boundary catastrophe in the Maastrichtian type area. Abstract book GC5-Mass-15

European Geosciences Union General Assembly 2018. Vienna

- 1) Dehais et al. https://meetingorganizer.copernicus.org/EGU2018/EGU2018-15135.pdf
- 2) Smit et al.https://meetingorganizer.copernicus.org/EGU2018/EGU2018-11331-1.pdf
- 3) De Graaff et al.https://meetingorganizer.copernicus.org/EGU2018/EGU2018-8314.pdf
- 4) Kaskes et al.https://meetingorganizer.copernicus.org/EGU2018/EGU2018-8190.pdf

Geological Belgica 2018 Leuven

- **Déhais, T., Kaskes, P., De Graaff, S.J., Goderis, S., Claeys, Ph**., Comparative petrographic geochemical, isotopic characterisation of distal ejecta, Abstract volume p. 4-5
- **De Graaff, S.J.,** Vandijk, R., **Kaskes, P., Déhais, T., Goderis, S., Claeys, Ph**., Making sense of destruction: Geochemistry of the Chicxulub impact melt rocks and granitoid target, recovered during IODP-ICDP Expedition 364, Abstract volume p. 2-3
- **Kaskes, P., De Graaf, S.J.**, Op de Beek, S., **de Winter, N., Déhais, T.,** Smit, J., **Goderis, S., Claeys, Ph.**, Mode of emplacement of the Chicxulub breccia, Abstract volume p. 1-2

10th International Symposium Cephalopods Present and Past, April 2018, Fez, Morocco

- **Goolaerts, S.** Nautiloid turnover across the Cretaceous/Paleogene Boundary: Chicxulub impact, Deccan volcanism and Europa as a key? Münstersche Forschungen zur Geologie und Paleontologie 110, 30.

International Paleontological Conference,July 2018, Paris, France

- **Goolaerts, S., Godefroit, P.** A double 'whammy' for ammonites and dinosaurs: fake news or the real deal**.**

6. PUBLICATIONS

As of 1.10.2022, a total of **41** papers were published in international peer-reviewed journals based on this BELSPO funding, including 1 Science, 2 Nature, and 15 by a first author directly supported by this BELSPO project. The majority of these manuscripts are in open access (either gold, green, or via pre-print and authors version, or placed onto an open access platform like that of the RBINS https://library.naturalsciences.be/pdfs-open-access/welcome, or VUB PURE https://researchportal.vub.be/en/organisations/analytical-environmental-geo-chemistry/publications/).

Submitted:

Senel, C. B., Kaskes, P., Temel, O., Vellekoop, J., Goderis, S., DePalma, R., Prins, M., **Claeys, P., & Karatekin, O.** (2022). Another one bites the dust: Photosynthetic collapse after the Chicxulub impact. Nature Geoscience (under review). https://doi.org/10.21203/rs.3.rs-1859469/v1.

De Graaff, S.J., Ross, C.H., Feignon, J-G., **Kaskes, P.,** Gulick, S.P.S., **Goderis, S., Déhais, T.,** Debaille, V., Ferrière, L., Koeberl, C., Mattielli, N., Stockli, D., **Claeys, Ph**., The Chicxulub structure reveals first in-sity Jurassic aged basement of the Yucatán Peninsular, Mexico, Lithos (under review).

2022 (13)

(41) **Déhais, T.,** Chernonozhkin, S., **Kaskes, P., de Graaff, S.J.,** Debaille, V., Vanhaecke, F., **Claeys, Ph., Goderis, S.**, Resolving impact volatilization and condensation from target rock mixing and hydrothermal overprinting within the chicxulub impact structure, *Geosciences Frontiers*, #101401, 2022, https://doi.org/10.1016/j.gsf.2022.101410, [IF 6.854]

(40) **de Graaff, S., Kaskes, P., Dehais, T., Goderis, S.,** Debaille, V., Ross, C., Gulick, S.P., Feignon, J.G., Ferriere, L., Koeberl., C., Smit, J., Mattielli, N., **Claeys, Ph.,** New insights into the formation and emplacement of impact melt rocks within the Chicxulub impact structure, following the 2016 IODP-ICDP Expedition 364, *Geological Society of America Bulletin*, 134 (1-2): 293–3152022, https://doi.org/10.1130/B35795.1, [IF 4.368]

(39) de la Parra, F., Jaramillo, C., **Kaskes P., Goderis, S., Claeys, Ph.,** Villasante-Marcos, V., Bayona, G., Hatsukawa, Y., Caballero, D., Unravelling the record of a tropical continental Cretaceous-Paleogene boundary in northern Columbia, South America, *Journal of South American Earth Sciences*, 2022, https://doi.org/10.1016/j.jsames.2022.103717, [IF 2.093]

(38) Feignon, J-G., Schulz, T., Ferrière, L., **Goderis, S., de Graaff, S.J., Kaskes, P., Déhais, T., Claeys, Ph**., Koeberl, C., Search for a meteoritic component within the impact melt rocks of the Chicxulub impact structure peak ring, Mexico, *Geochimica Cosmochimica Acta*, 323, 74-101, 2022, https://doi.org/10.1016/j.gca.2022.02.006, [IF 5.101]

(37) **Kaskes, P., de Graaff, S.J.,** Feignon*, J-G, **Déhais, T., Goderis, S.,** Ferriere, L., Koeberl, C., Smit, J., Wittman, A., Gulick, S.P.S., Debaille, V., Mattielli, N., **Claeys, Ph**., Formation of the crater suevite sequence from the Chicxulub crater peak-ring: A petrographic geochemical and sedimentologycal characterisation, *Geological Society of America Bulletin*, 134, (3-4) 895-927, 2022, https://doi.org/10.1130/B36020.1, [IF 4.368]

(36) Ross, C.H., Stockli, D.F., Rasmussen, C., Gulick, S.P.S., **de Graaf, S., Claeys, Ph.,** Zhao, J., Xiao, L., Pickersgill, A.E., Schmieder, M., Kring, D., Wittman, A., Morgan, J.V., Evidence of Carboniferous arc magmatism preserved in the Chicxulub impact structure, *Geological Society of America Bulletin*, 134 (1-2), 241-260, 2022, https://doi.org/10.1130/B35831.1, [IF 4.368]

(35) Vancoppenolle, I, **Vellekoop, J.,** Doubrawa, M., **Kaskes, P., Sinnesael, M.,** Jagt, J.W.M., **Claeys, Ph.** Speijer, R.P., The benthic foraminiferal responses to the mid-Maastrichtian event in NW-European Chalk sea of the Maastrichtian type area, Netherlands Journal of Geosciences, 101, e12, https://doi.org/10.1017/njg.2022.10, [3.263]

(34) **Vellekoop*, J., Kaskes, P., Sinnesael, P., Huygh, J**., **Déhais, T.,** Jagt, J.W.M., Speijer, R.P., **Claeys, Ph.,** A new age model and chronostratigraphic framework for the Maastrichtian type area (southeastern Netherlands, northeastern Belgium), *Newsletters on Stratigraphy*, 2022, doi:10.1127/nos/2022/0703 [IF 2.83]

(33) Fernando, B., Wójcicka, N., Maguire, R., Stähler, S. C., Stott, A. E., Ceylan, S., Charalambous, C., Clinton, J., Collins, G. S., Dahmen, N., Froment, M., Golombek, G., Horleston, A., **Karatekin, O.**, … & Daubar, I. J. (2022). Seismic constraints from a Mars impact experiment using InSight and Perseverance. *Nature Astronomy*, *6*(1), 59-64.

(32) Michel, P., Küppers, M., Bagatin, A. C., Carry, B., Charnoz, S. …, **Karatekin, O.** ... & Carnelli, I. (2022). The ESA Hera Mission: Detailed Characterization of the DART Impact Outcome and of the Binary Asteroid (65803) Didymos. *The Planetary Science Journal*, *3*(7), 160.

(31) Agrusa, H. F., Ballouz, R., Meyer, A. J., Tasev, E., Noiset, G., **Karatekin, O.**, ... & Hirabayashi, M. (2022). Rotation-induced granular motion on the secondary component of binary asteroids: Application to the DART impact on Dimorphos. *Astronomy & Astrophysics*, *664*, L3.

(30) Richardson, D. C., Agrusa, H. F., Barbee, B., … **Karatekin, O.** ... & Zhang, Y. (2022). Predictions for the Dynamical States of the Didymos System before and after the Planned DART Impact. *The Planetary Science Journal*, *3*(7), 157.

(29) **Temel, O., Senel, C. B.**, Spiga, A., Murdoch, N., Banfield, D., & **Karatekin, O.** (2022). Spectral analysis of the Martian atmospheric turbulence: InSight observations. *Geophysical Research Letters*, e2022GL099388.

2021 (9)

(28) Cockell, C., Schaeffer, B., Wuchter, C., Coolen, M.J.L., Grice, K., Schneiders, L., Morgan, J., Gulick, S., Wittmann, A., Lofi, J. Christeson, G., Kring, D., Whalen, M., Bralower, T., Osinski, G., **Claeys, Ph., Kaskes, P., de Graaff, S., Dehais, T., Goderis, S.,** Hernandez, N., Nixon, S., Shaping of the present-day deep biosphere at Chicxulub by the impact catastrophe that ended the Cretaceous, *Frontiers in Microbiology*, 12, 1413, 2021, doi: 10.3389/fmicb.2021.668240 [IF 4,076]

(27) Feignon, J-G., **de Graaff, S.J.,** Ferriere, L., **Kaskes, P., Déhairs, T., Goderis, S., Claeys, Ph**. Koeberl, C., Chicxulub impact structure, IODP-ICDP expedition 364 drill core: Geochemistry of the granite basement, *Meteoritics & Planetary Science*, 1-31, 2021, https://doi.org/10.1111/maps.13705 [IF 2.863]

(26) Gale, A., Jagt, J.WM., **Goolaerts, S.,** Cirripedes (Thoracica, Crustacea) from the Maastrichtian of Kalaat Senan, Tunisia. Cretaceous Research, 118, 104650, 2021, https://doi.org/10.1016/j.cretres.2020.104650 [IF 2.01] Not OA (but with 50 days free access from publisher following online publication)

(25) **Goderis, S.,** Sato, H., Ferrière, L., Schmitz, B., Burney, D**., Kaskes, P., Vellekoop, J.,** Wittmann, A., Schulz, T., Chernonozhkin, S., **Claeys, Ph, de Graaff, S.J., Déhais, T., de Winter**, N.J., Elfman, M., Feignon, J-G., Ishikawa, A., Koeberl, C., Kristiansson, P., Neal, C.R., Owens, J.R., Schmieder, M., **Sinnesael, M.,** Vanhaecke, F., Van Malderen, S.J.M., Bralower, T., Gulick, S.P.S., Kring, D.A., Lowery, C.M., Morgan, J.V., Smit, J., Whalen, M.T., and the IODP-ICDP Expedition 364 Scientists, Globally distributed iridium layer preserved within the Chicxulub impact structure, *Science Advances*, 7, 9, eabe3647, 2021, https://doi.org/10.1126/sciadv.abe3647 [IF 16.446]

(24) Hoffmann, R., Slattery, J., Kruta, I., Linzmeier, B.J., Lemanis, R.F., Mironenko, A., **Goolaerts, S.,** Klug, C., De Baets, K., Peterman, D.J., Recent advances in Heteromorph ammonoid paleobiology. Biological Reviews, 96, 576-610, 2021, https://doi.org/10.1111/brv.12669 [IF 14.69]

(23) **Kaskes*, P., Déhais*, T., de Graaff*, S.J., Goderis, S., and Claeys, Ph**., 2021, Micro–X-ray fluorescence (µXRF) analysis of proximal impactites: High-resolution element mapping, digital image analysis, and quantifications, in Reimold, W.U., and Koeberl, C., eds., Large Meteorite Impacts and Planetary Evolution VI: Geological Society of America Special Paper 550, p. 1–36, 2021, https://doi.org/10.1130/2021.2550(07).

(22) Zhao, J., Xiao, L., Xiao, Z., Morgan, J.V., Osinski, G.R., Neal, C.R., Gulick, S.P.S., Riller, U., **Claeys, Ph.**, Zhao, S., Prieur, N.C., Nemchin, A., Yu., Shuoran, and IODP 364 Sience Party, Shock-deformed zircon from the Chicxulub impact crater and implications for cratering process, *Geology*, 49, 1-4, 2021, https://doi.org/10.1130/G48278.1 [IF 5.412]

(21) **Senel, C. B., Temel, O**., Lee, C., Newman, C. E., Mischna, M. A., Muñoz-Esparza, D., ... & **Karatekin, O.** (2021). Interannual, seasonal and regional variations in the Martian convective boundary layer derived from GCM simulations with a semi-interactive dust transport model. Journal of Geophysical Research: Planets, 126(10), e2021JE006965.

(20) **Temel, O., Karatekin, O.,** Mischna, M. A., **Senel, C. B**., Martínez, G., Gloesener, E., & Van Hoolst, T. (2021). Strong Seasonal and Regional Variations in the Evaporation Rate of Liquid Water on Mars. Journal of Geophysical Research: Planets, 126(10), e2021JE006867.

2020 (5)

(19) **de Winter* N.J.,** Ullmann, C., Sørensen, A.M., Thibault N., **Goderis, S.,** Van Malderen, SJ.M., **Snoeck, C., Goolaerts, S.,** Vanhaecke, F., **Claeys, Ph.,** Shell chemistry of the boreal Campanian bivalve *Rastellum diluvianum* (Linnaeus, 1767) reveals temperature seasonality, growth rates and life cycle of an extinct Cretaceous oyster. *Biogeosciences*, 17, 2897-2922, 2020, https://doi.org/10.5194/bg-17-2897-2020, [IF 4.194]

(18) **de Winter*, N., Goderis, S.,** Van Malderen, , S.J.M., **Sinnesael, M., Vansteenberge, S., Snoeck, C., Belza, J.,** Vanhaecke, F., **Claeys, Ph.** Subdaily-Scale Chemical Variability in a Torreites Sanchezi Rudist Shell: Implications for Rudist Paleobiology and the Cretaceous Day-Night Cycle, *Paleoceanography and Paleoclimatology*, 35, e2019PA003723, 2020, https://doi.org/10.1029/2019PA003723, [IF 3.09]

(17) Kring, D. A., Tikoo, S. M., Schmieder, M., Riller, U., Rebolledo-Vieyra, M., Simpson, S. L., Osinski, G. R., Gattacceca, J., Wittmann, A., Verhagen, C. M., Cockell, C. S., Coolen, M. J. L., Longstaffe, F. J., Gulick, S. P. S., Morgan, J. V., Bralower, T. J., Chenot, E., Christeson, G. L., **Claeys, P.,** Ferrière, L. & others, Probing the hydrothermal system of the Chicxulub impact crater, *Science Advances*. 6, 22, 1-8., eaaz3053, 2020, DOI: 10.1126/sciadv.aaz 3053. [IF 12.804]

(16) **Vellekoop, J.,** Van Tilborgh, K.H., Van Knippenberg, P., Jagt, J.W.M., Stassen, P., **Goolaerts, S.,** Speijer, R.P.,2020. Type Maastrichtian Gastropod faunas showing rapid ecosystem recovery following the Cretaceous/Paleogene boundary catastrophe. Palaeontology 63(2), 349-367. [IF: 2.632] Not OA

(15) Zhao, J., Xiao, L., Gulick, S. PS., Morgan, J. V., Kring, D., Urrutia-Fucugauchi, J., Schmieder, M., de Graaff, S. J., Wittmann, A., Ross, C. H., **Claeys, P.,** Pickersgill, A., Kaskes, P., Goderis, S., Rasmussen, C., Vajda, V., Ferriere, L., Feignon, JG., Chenot, E., Perez-Cruz, L., Sato, H., Yamaguchi, K., and IODP-ICDP Expedition 364 Science Party, Geochemistry, geochronology and petrogenesis of Maya Block granitoids and dikes from the Chicxulub Impact Crater, Gulf of Mexico: Implications for the assembly of Pangea, Gondwana Research, 82, 128-150, 2020, https://doi.org/10.1016/j.gr.2019.12.003 [IF 6.478]

2019 (5)

(14) Gulick, S.P.S, Bralower, T., Ormo, J., Hall, Brendon, Grice, K., Schaefer, B., Lyons, S., Freeman, K. H., Morgan, J. V., Artemieva, N., **Kaskes, P., de Graaff, S.J.,** Whalen, M.T., Collins, G., Tikoo, S.M., Verhagen, C., Christeson, G., **Claeys, Ph**., Coolen, M.J.L., Goderis. S., Goto, K., Grieve, R.A.F., McCall, N., Osinski, G. R., Auriol, R.S.P., Riller, U., Smit, J., Vajda, V., Wittmann, A., and the Expedition 364 Scientists, The first day of the Cenozoic, Proceedings of the National Academy of Sciences USA, 116, (39) 19342-19351, 2019, www.pnas.org/cgi/doi/10.1073pnas.1909479116 [IF 9.5804]

(13) Lowery, C. M., Morgan, J. V., Gulick, S. P. S., Bralower, T. J., Christeson, G. L., Chenot, E., **Claeys, Ph.** & Expedition 364 Scientists, Ocean drilling perspectives on meteorite impacts, Oceanography, 32, 1, p. 120-134, 2019, https"//doi.org/10.5670/oceanog.2019.133, [IF 3.883]

(12) Timms, N. E., Pearce, M. A., Erickson, T. M., Cavosie, A. J., Rae, A. S. P., Wheeler, J., Wittmann, A., Ferri.re, L., Poelchau, M. H., Tomioka, N., Collins, G. S., Gulick, S. P. S., Rasmussen, C., Morgan, J. V., Chenot, E., Christeson, G. L., **Claeys, Ph.** & IODP-ICDP Expedition 364 Scientists, New shock microstructures in titanite (CaTiSiO5) from the peak ring of the Chicxulub impact structure, Mexico, Contributions to Mineralogy and Petrology, 174, 5, 38, 1-22, 2019, doi.org/10.1007/s00410-019-1565-7, [IF 3.230]

(11) **Sinnesael*, M.,** Montanari, A., Frontalini, F., Coccioni, R., Gattacceca, J., **Snoeck*, C.,** Wegner, W., Koeberl, C., Morgan, L. E., **de Winter, N.,** DePaolo, D.J., **Claeys, Ph.,** Multiproxy Cretaceous-Paleogene boundary event stratigraphy: An Umbria-Marche basinwide perspective, in 250 Million Years of Earth History in Central Italy: Celebrating 25 Years of the Geological Observatory of Coldigioco, Geological Society of America Special Papers 542, 6, https://doi.org/10.1130/2019.2542(07), ISBN (Electronic): 9780813795423

(10) Urrutia-Fugugauchi, J., Perez-Cruz, L., Morgan, J., Gulick, S., Wittmann, A., Lofi, J., **Claeys, Ph**. and IODPICDP 364 Exp. Science Party, Peering inside the peak ring of the Chicxulub Impact Crater—its nature and formation mechanism, Geology Today, 35, 2, 68-72, 2019.

2018 (5)

(9) Lofi, J., Smith, D., Delahunty, C., Le Ber, E., Brun, L., Henry, G., Paris, J., Tikoo, S., Zylberman, W., Pezard, P. A., C.l.rier, B., Schmitt, D. R., Nixon, C., Gulick, S. P. S., Morgan, J. V., Chenot, E., Christeson, G. L., **Claeys, P.** & IODP-ICDP Expedition 364 Science Party, Drilling-induced and logging related features illustrated from IODP-ICDP Exp. 364 downhole logs and borehole imaging tools, Scientific Drilling, 24, 1-13, 2018, DOI: 10.5194/sd-24-1-2018

(8) Lowery C. M., Bralower, T. J., Owens, J. D., Rodr.guez-Tovar, F. J., Jones, H., Smit, J., Whalen, M. T., **Claeys, Ph**., Farley, K, Gulick, S. PS., Morgan, J. V., Green, S., Chenot, E., Christeson, G. L., Cockell, C. S., Coolen M. JL., Ferri.re, L., Gebhardt, C., Goto, K., Kring, D. A., Lofi, J., Ocampo-Torres, R., Perez-Cruz L., Pickersgill, A. E., Poelchau, M., Rae, A. S. P., Rasmussen, C., Rebolledo-Vieyra, M., Riller, U., Sato, H., Tikoo, S. M., Tomioka, N., Urrutia-Fucugauchi, J., **Vellekoop, J.,** Wittmann, J., Xiao, L., Yamaguchi, K. E., Zylberman, W., Life Recovered Rapidly at Impact Site of Dino-Killing Asteroid, Nature in press, published on May 30, 2018.

(7) Christeson, G., L., Gulick, S., Morgan, P. S., Gebhardt, C. Kring, D. A., Le Ber, J Lofi, J., Nixon, C., Poelchau, M., Rae A., SP., Rebolledo-Vieyra, M., Riller, U., Schmitt, D., R., Wittmann, A., Bralower, T., J., Chenot, E., **Claeys, Ph**., Cockell, C., S., Coolen, M., JL., Ferri.re, L., Green, S., Goto, K., Jones, H., Lowery, C. M., Mellett, C., Ocampo-Torres, R., Perez-Cruz, L., Pickersgill, A. E., Rasmussen, C., Sato, H., Smit, J., Tikoo, S., M., Tomioka, N., Urrutia-Fucugauchi, J., Whalen, M. T., Xiao, L., Yamaguchi, K.E., Extraordinary rocks from the peak ring of the Chicxulub impact crater: P-wave velocity, density, and porosity measurements from IODP/ICDP Expedition 364, Earth and Planetary Science Letters, 495, 1-11, 2018, https://doi.org/10.1016/j.epsl.2018.05.013 [IF 4.409]

(6) Riller, U., Poelchau, M. H., Rae, A. S. P., Schulte, F. M., Collins, G. S., Melosh, H. J., Grieve, R. A. F., Morgan, J. V., Gulick, S. P. S., Lofi, J., Diaw, A., McCall, N., Kring, D. A., Green, S. L., Chenot, E., Christeson, G. L., **Claeys, P.,** Cockell, C. S., Coolen, M. J. L., Ferri.re, L. & 20 others, Rock fluidization during peak-ring formation of large impact structures, Nature, 562, 511-518, 2018, doi:10.1038/s441586-018-0607-z, [IF 40.137]

(5) **Sinnesael, M., de Winter, N., Snoeck, C.**, Montanari, A., **Claeys, Ph.,** An integrated pelagic carbonate multiproxy study using portable X-ray fluorescence (pXRF): Maastrichtian strata from the Bottaccione Gorge, Gubbio, Italy, Cretaceous Research, 91, 20-32, 2018, https://doi.org/10.1016/j.cretres.2018.04.010 [IF 2.01]

2017-2016 (4)

(4) **Belza*, J., Goderis, S**., Montanari, A., Vanhaecke, F., and **Claeys, Ph.,** Petrography and geochemistry of distal spherules from the K-Pg boundary in the Umbria-Marche region (Italy) and their origin as fractional condensates and melts in the Chicxulub impact plume, Geochimica et Cosmochimica Acta, 202, 231-263, 2017, https://doi.org/10.1016/j.gca.2016.12.018, [IF 4.847].

(3) Kring, D. A., **Claeys, Ph**., Gulick, S. P., Morgan. J. V., Collins, G., S., Chicxulub and the Exploration of Large Peak-Ring Impact Craters through Scientific Drilling, GSA Today, 27, 10, 4-8, 2017 (Invited), https://www.geosociety.org/gsatoday/science/G352A/GSATG352A.pdf.

(2) Morgan, J., Gulick, S., Mellett, C.L., Green, S.L., Claeys, Ph. and the Expedition 364 Scientists, Chicxulub: Drilling the K-Pg Impact Crater. Proceedings of the International Ocean Discovery Program, 364: College Station, TX (International Ocean Discovery Program), 30 December 2017. https://doi.org/10.14379/iodp.proc.364.2017, ISSN: World Wide Web: 2377-3189,

(1) Morgan, J., Gulick, S., Bralower, T., Chenot, E., Christeson, G., **Claeys, Ph**., and 33 IODP cruise members, The formation of peak rings in large impact craters, Science, 354, 6314, 878-882, 2016. [IF 34.661]

7. ACKNOWLEDGEMENTS

Thanks to VUB-AMGC David Verstraeten isotope lab manager for support during analyses. IODP Bremen and Texas A&M core repository are acknowledged for access and assistance during sampling. We also thank the “follow up committee”, especially Profs Jan Smit and Jo Morgan for frequent and constructive discussion.

We warmly thank BELSPO, the program manager, and staff for supporting this work.